LBL-29472
UC-414

Lawrence Berkeley Laboratory
UNIVERSITY OF CALIFORNIA

Accelerator & Fusion
Research Division

RFQ's—An Introduction

J.W. Staples

September 1990

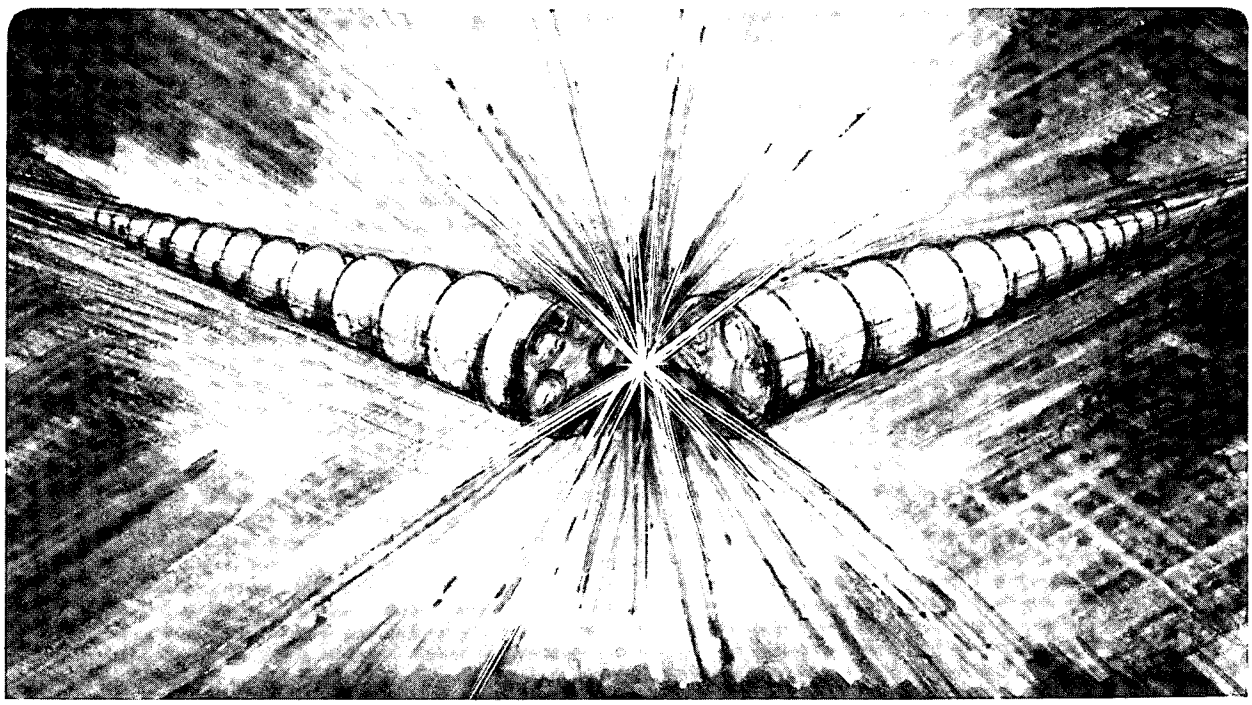

Prepared for the U.S. Department of Energy under Contract Number DE-AC03-76SF00098.

DISCLAIMER

LBL-29472

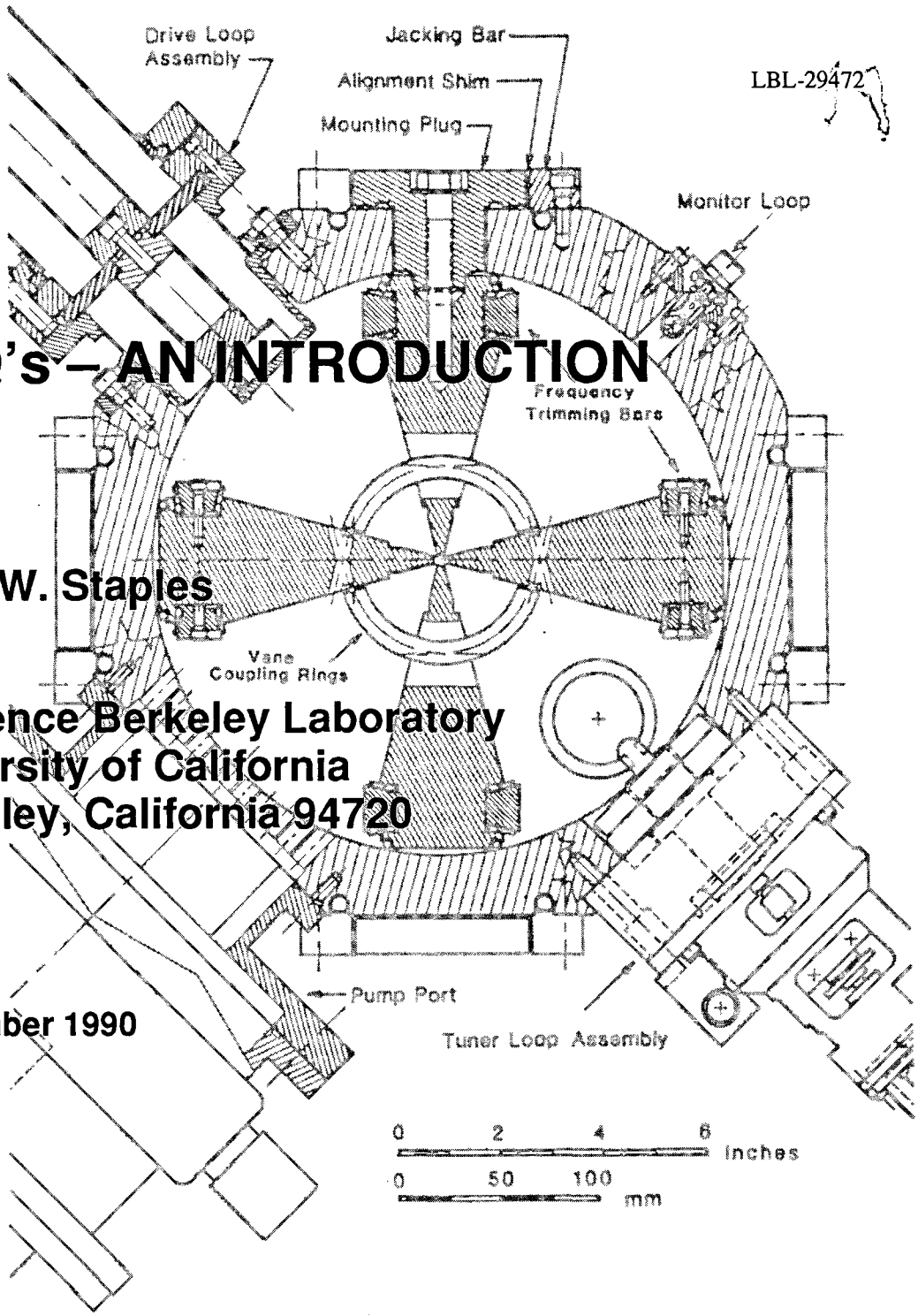

RFQ's – AN INTRODUCTION

John W. Staples

Lawrence Berkeley Laboratory
University of California
Berkeley, California 94720

September 1990

This work supported by the Director, Office of Energy Research, Office of High Energy and Nuclear Physics, Nuclear Science Division, U. S. Department of Energy under contract number DE-AC03-76SF00098.

RFQs — An Introduction

John W. Staples
Lawrence Berkeley Laboratory, University of California, Berkeley, CA 94720

Contents

RFQs — An Introduction

John W. Staples
Lawrence Berkeley Laboratory, University of California, Berkeley, CA 94720

1 Introduction

This chapter is a practical introduction to RFQs (radio frequency quadrupole accelerators). My aim is to give you enough information about RFQs so you can understand their principles of operation and their strengths and weaknesses.

Invented in the USSR by Teplyakov and Kapchinskii [1] in 1970, the RFQ was first brought to the attention of Western physicists by Joe Manca [2] at Los Alamos. Their first RFQ was a small and highly successful 425-MHz proton accelerator, a "proof of principle" device. The RFQ has dominated the area of low energy linacs (linear accelerators) in the last few years.

The RFQ is a low-velocity, high-current linear accelerator with high capture efficiency that can accelerate ion species from protons to uranium. Ion sources need only to operate at relatively low extraction and preacceleration voltages to inject the RFQ. The RFQ output energy is well matched to the input energy requirement of linear accelerators that accelerate ions to higher energy, and has been included in most new linac designs.

Many laboratories have also adopted the RFQ as a "front end" accelerator in their synchrotron injectors. The RFQ has almost replaced the large 750-kV air-insulated Cockcroft-Walton (C-W) dc preaccelerator found at older proton synchrotron injectors. The small, compact and reliable RFQ provides operational cost savings over the large C-W sets and allows the ion source to be operated closer to ground potential, reducing the size of the preinjector and improving access to the ion source.

I will first give a brief overview of the theory of the operation of the RFQ.

2 RFQ Characteristics

The RFQ, as shown in Figure 1, is a focusing (or transport) structure [3] to which acceleration is added as a perturbation. Other linac types impose focusing onto an accelerating structure. This fundamental focusing attribute of the RFQ gives rise to many advantages in low-velocity acceleration, as will be explained below.

A time-varying transverse quadrupole electric field forms an *alternating gradient* focusing channel. The acceleration process, including longitudinal focusing, results in transverse defocusing of the beam as a three-dimensional potential well cannot be established by static fields. Transverse focusing must be introduced to avoid particle loss during the accelerating process. The alternating-gradient

transverse focusing field results in stability in all three spatial dimensions given an appropriate choice of parameters.

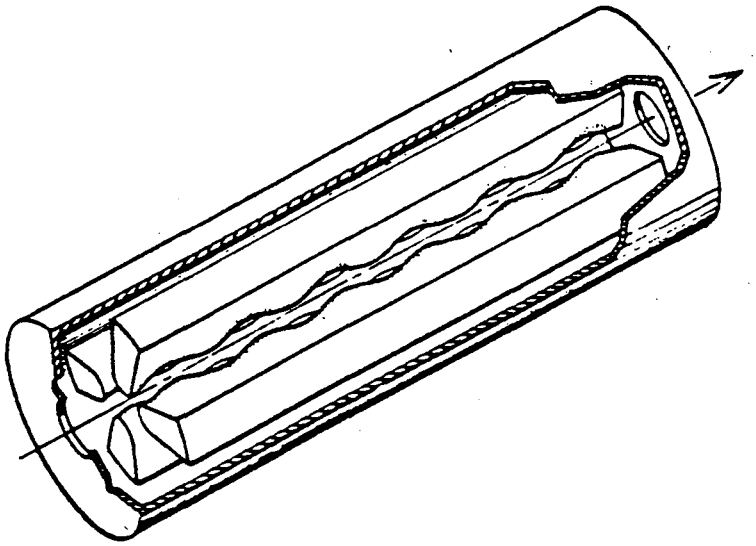

Figure 1: Four-Vane RFQ Structure

2.1 Bunching

The beam accelerated in a linac must first be formed into bunches at the operating frequency (or a subharmonic) before it can be accelerated by the longitudinal rf field in the structure. The bunching process in other linacs usually discards 30 to 50% of the beam. The RFQ uses *adiabatic bunching* to gently gather and accelerate nearly 100% of the beam from the ion source, a distinct advantage for rare ion species such as polarized ions or high-charge-state heavy ions.

Acceleration is produced by perturbing the rf quadrupole structure to generate longitudinal fields which bunch and accelerate the beam. Adiabatic bunching requires that the longitudinal field increase slowly along the axis, gently forming the bunch with minimum loss and minimum accumulated longitudinal emittance. The longitudinal field E_ℓ is determined by the geometry of the vane tip, and can range down to zero. Any arbitrary longitudinal field law can thus be established and optimized to provide efficient bunching and capture.

2.2 RFQ Energy Limit

The RFQ is a *Sloan-Lawrence* accelerator (described below). The acceleration efficiency (longitudinal shunt impedance) of a Sloan-Lawrence accelerator decreases with velocity. This, along with a field distribution error sensitivity which goes as the square of the length, sets a practical upper limit to the output energy, in MeV/n, of approximately $2q/A$ MeV/n, where q is the charge state of the ion

and A is the mass in amu. Fortunately, the typical RFQ output beam energy is compatible with the injection energy requirements of higher-energy linacs.

3 Low Velocity Accelerators

Direct current accelerators, such as the Cockcroft-Walton, accelerate particles through a dc potential drop of V, the final energy being $W = qV$, where q is the ion charge. The practical upper limit for air insulated accelerators is about 10^6 volts.

Linacs extend this limit by periodically applying a radio-frequency field of frequency f to the accelerated particle. In free space, the particle would just oscillate back and forth without being accelerated. By the use of *drift tubes* in the structure, the spatial field distribution is modified, producing a net acceleration. The drift tubes shield the ion on the negative half of the rf cycle, preventing deceleration.

3.1 Sloan-Lawrence Accelerators

Low velocity linacs can be divided into two groups: *Sloan-Lawrence* and *Alvarez* accelerators, as shown in Figure 2. The Sloan-Lawrence accelerator places al-

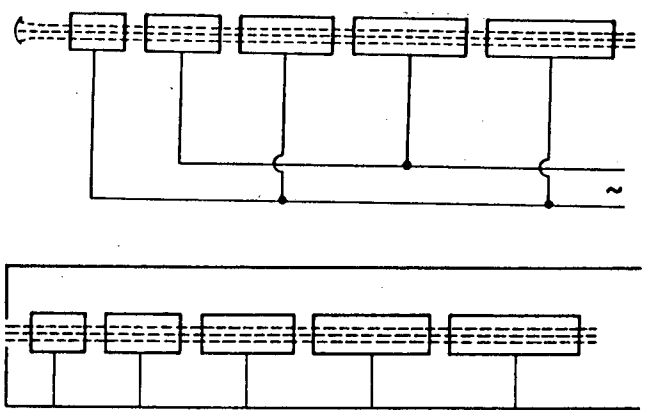

Figure 2: Sloan-Lawrence (top), and Alvarez Accelerator

ternately charged drift tubes along the axis with the gaps an odd multiple of $\beta\lambda/2$ apart, where $\beta = v/c$ is the normalized particle velocity and $\lambda = c/f$ is the free-space rf wavelength. The fields in successive gaps alternate in polarity, with half accelerating and half decelerating. By the time an ion has progressed

from the center of one gap to the next, the rf phase has advanced by $\pi/2$ and the decelerating field in the next gap has reversed. The bunches are spaced by $\beta\lambda$.

3.2 Alvarez Accelerators

Alvarez accelerators look superficially the same, but operate by exciting a longitudinal electric field in a cavity. Charges on the ends of the drift tubes are produced by displacement currents, and the field in all gaps has the same polarity. The spacing between gaps is $n\beta\lambda$, and the bunches are again spaced by $\beta\lambda$.

Sloan-Lawrence accelerators were first operated in the 1920s [4] and are usually applied to acceleration of very-low-velocity particles. The Alvarez structure [5] was proposed in the 1940s and is most efficient in a higher energy range. Proton linacs use the Alvarez structure in the range of approximately 0.5 to 100 MeV. Below that range, RFQs are more appropriate, and above that range alternate structures are used because they have a higher acceleration efficiency.

Focusing in either the Sloan-Lawrence or the Alvarez linac is usually provided by magnetic quadrupoles placed in the drift tubes. To a first approximation, the integrated quadrupole field is constant along the entire accelerator. Since each drift tube length is proportional to β, the normalized ion velocity, the early drift tubes will be short and the required quadrupole gradient will be high. This is the most significant determinant of the injection energy of Alvarez or Sloan-Lawrence linacs, particularly for heavy ions.

4 Alternating-Gradient Focusing

As the RFQ is essentially an alternating-gradient focusing channel with acceleration added as a perturbation to the fundamental structure, it is appropriate to start with a discussion of strong focusing.

It is well known from geometric optics that a periodic sequence of focusing and defocusing lenses of appropriate and equal strengths provides net focusing for certain values of lens spacing and strength. The principle of alternating-gradient (strong) focusing is based on extending this idea, incorporating a sequence of focusing and defocusing lenses to transport and contain a beam.

Among the lens options used in beam optics are solenoids and quadrupoles. Solenoids are relatively weak and require large, power-consuming magnets. Quadrupoles offer stronger focusing, but in only one transverse plane; the beam in the other plane is defocused. A sequence of quadrupoles of alternating polarity will focus in both planes, generally with less power consumption than solenoids with equivalent focusing strength.

Besides magnetic quadrupoles, electrostatic focusing can also be used. The magnetic quadrupole is more effective at higher velocity as the electromagnetic coupling, $\mathbf{v} \times \mathbf{B}$, scales with velocity, with electrostatic focusing being more effective at low β.

4.1 Electrostatic Quadrupoles

Figure 3 shows the geometry of an electrostatic quadrupole with electrodes at potential $\pm V_0$ and minimum radius a. As there are no free charges within the

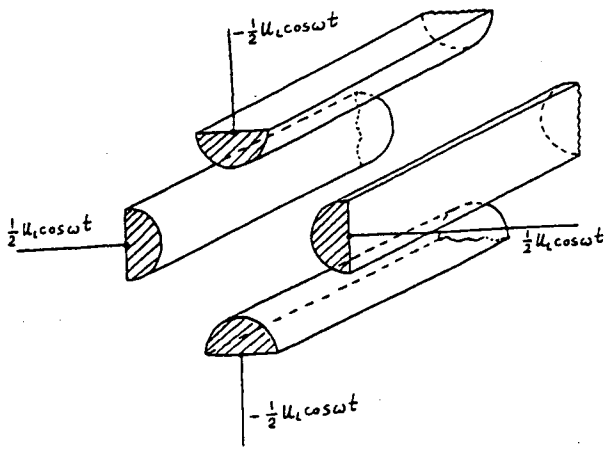

Figure 3: Electrostatic Quadrupole

space bounded by the electrodes (we are ignoring space-charge for the moment), the potential ϕ_E that satisfies $\nabla^2\phi_E = 0$ is given by $\mathbf{E} = -\nabla\phi_E$. The solution near the axis which satisfies the boundary conditions is

$$E_x = g_0 x, \quad E_y = -g_0 y \tag{1}$$

where $g_0 = V_0/a^2$. The transverse equations of motion are then

$$m\ddot{x} = +qeg_0 x, \tag{2}$$

$$m\ddot{y} = -qeg_0 y \tag{3}$$

where q is the number of electronic charges e on the particle. The solutions in the two planes are sinusoidal and bounded, or hyperbolic and unbounded.

4.2 Alternating-Gradient Quadrupoles

If the voltage on the electrodes has a time dependence

$$V(t) = V_0 \sin(\omega t), \tag{4}$$

then for certain ranges of V_0 the transverse motion is bounded in both transverse planes.

The free-space wavelength λ corresponding to frequency $f = \omega/2\pi$ is $\lambda = c/f$. The fundamental focusing period length $\beta\lambda$ is the distance an ion of normalized velocity $\beta = v/c$ travels in one rf period. This length is the focusing period of the

alternating focusing structure, and is unrelated to the scallops seen on the vane surfaces of RFQs.

The equation of transverse motion

$$m\ddot{x} = qeE_x = qeg_0 \sin(\omega t)x \tag{5}$$

can be expressed as

$$\beta^2\lambda^2\frac{d^2x}{dz^2} = B_0 \sin(kz)x, \tag{6}$$

where $k = 2\pi/\beta\lambda$ and the (unitless) focusing parameter B_0 is

$$B_0 = \frac{qeV}{mc^2}\frac{\lambda^2}{a^2}. \tag{7}$$

Later, we will redefine B slightly by introducing an additional focusing efficiency factor χ.

We will, at this point, introduce another term Δ, which models the transverse defocusing (also known as the rf defocusing) the ion experiences as it is accelerated. Δ is the (unitless) smoothed defocusing parameter which represents the change of the angle x' per displacement from the axis per focusing period. The actual defocusing is not continuous but is related to the rf phase and to the position of each particle within the bunch:

$$\Delta = \frac{\delta x'}{x}\frac{1}{\beta\lambda}. \tag{8}$$

The equation of motion with the defocusing term Δ is

$$\beta^2\lambda^2\frac{d^2x}{dz^2} = \Delta x \tag{9}$$

and the complete equation of motion with alternating-gradient focusing and rf defocusing becomes

$$\beta^2\lambda^2\frac{d^2x}{dz^2} = (B_0 \sin kz + \Delta)x. \tag{10}$$

This is Mathieu's equation, which has stable solutions for certain values of B_0 and Δ [1]. The stable orbits are solutions of Floquet's equation

$$x(z) = X(z)\sqrt{\beta(z)} \tag{11}$$

where $X(z)$ varies slowly over the focusing period $\beta\lambda$ and $\beta(z)$ (an unfortunate duplication of symbols for different variables) is periodic in $\beta\lambda$. $X(z)$ satisfies

$$\beta^2\lambda^2\frac{d^2X}{dz^2} + \sigma^2 X = 0, \tag{12}$$

[1] With the transformation $\pi z/\beta\lambda = v$, $B_0 = 2\pi^2 q$, $\Delta = -a\pi^2$, Eq. (10) is transformed to **20.1.1** in Abramowitz and Stegun [6].

where σ is the *tune*, or the rate of phase advance of a particle in the focusing structure, and is given by

$$\sigma^2 = \frac{B^2}{8\pi^2} + \Delta. \tag{13}$$

Figure 4 shows a typical trajectory embedded in the envelope of all possible stable trajectories. A specific trajectory is given by $e^{i\sigma z}$ modulated by a faster function $P(z)$, which is the envelope of all the orbits. The modulation depth of $P(z)$ depends on both B and Δ.

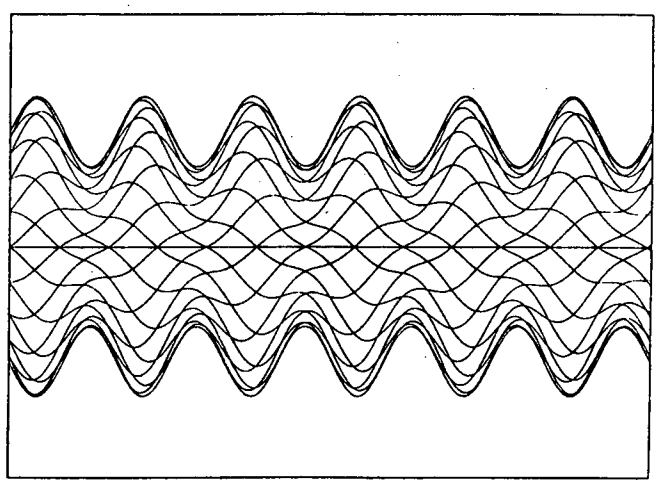

Figure 4: Individual Trajectory within Envelope

4.3 Transverse Stability

Figure 5 shows the limits of stability for values of the focusing strength B and rf defocusing strength Δ [7]. Also indicated on the graph are the tune, labeled σ, and the modulation depth Ψ^2, where the ratio of maximum to minimum beam radius is given by $\Psi = r_+/r_-$, where r_+ and r_- are the maximum and minimum envelope of the beam. As mentioned above, σ is the phase advance of a particle per focusing period $\beta\lambda$, producing the approximately sinusoidal transverse trajectory of the individual particle seen in Figure 4. The ratio $\Psi = r_+/r_-$ corresponds to the extrema of the function $\beta_\sigma(z)$.

The peak beam envelope amplitude r_+ is determined by the unnormalized emittance ϵ of the beam and the beam betatron amplitude $\hat{\beta}$:

$$(r_+)^2 = \epsilon\hat{\beta}. \tag{14}$$

The normalized betatron amplitude Γ_+ is related to the betatron amplitude $\hat{\beta}$ and the focusing period length $L_c = \beta\lambda$ by

$$\hat{\beta} = \Gamma_+ L_c. \tag{15}$$

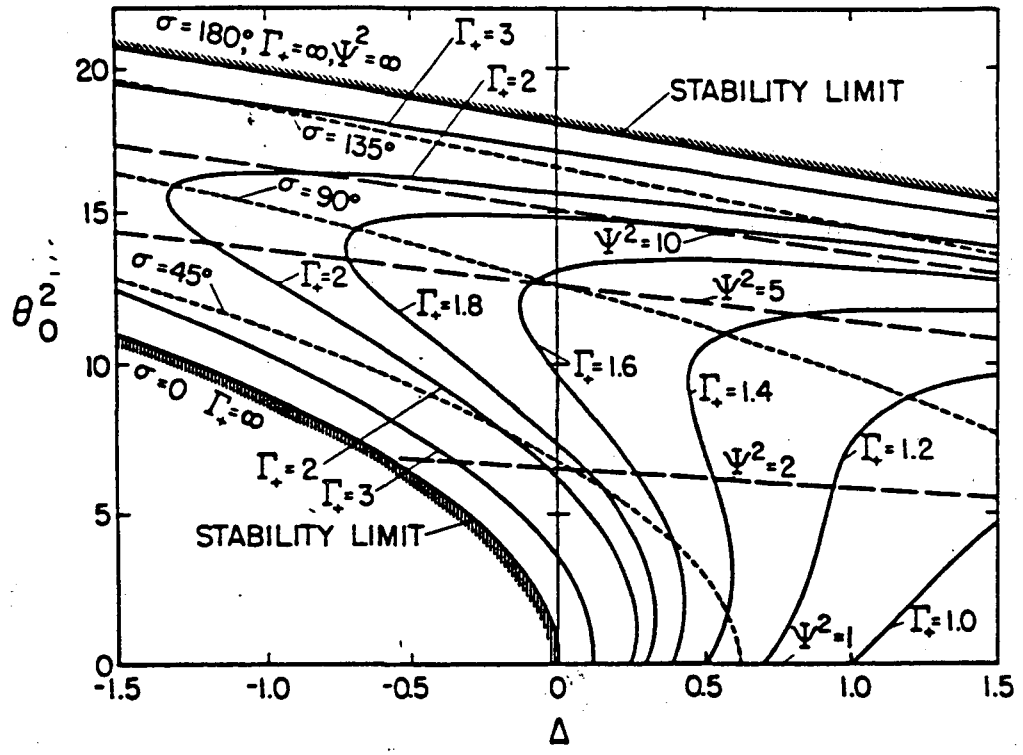

Figure 5: Transverse Stability Diagram

From Figure 5 we see that, for a certain range of focusing strength B, the orbits are stable. Phase stability during acceleration, discussed in the next section, results in transverse defocusing with $\Delta < 0$. We see that a minimum transverse focusing strength is also required for stability for $\Delta < 0$.

The lower stability boundary corresponds to the tune $\sigma = 0$. At that boundary, the peak envelope radius, proportional to $\Gamma_+^{1/2}$, becomes infinite. Similarly, at the upper stability boundary, the tune goes to 180° per $\beta\lambda$ focusing period, the trajectory is resonant with the period of the external focusing force, and the beam radius again becomes infinite.

The minimum beam size in the alternating quadrupole channel corresponds to the minimum value of Γ_+, which occurs at a phase advance *sigma* slightly less than 90° per $\beta\lambda$ period, with values of the focusing strength parameter B in the range of 10 to 15. It will be seen later that practical RFQ designs use values up to this (depending on many other factors, including space-charge effects, which require the flutter r_+/r_- to be minimized, and by peak electrode voltage, which is limited by sparking between the electrodes).

5 Acceleration

In this section, we will derive the equations of longitudinal motion and the limits of longitudinal stability.

5.1 Longitudinal Equation of Motion

We will follow the discussion of the longitudinal motion by Hereward [8], who in turn refers to Smith [9].

The longitudinal field on the axis of the RFQ is of the form

$$E_z = E_0 \sin(kz - \omega t) \tag{16}$$

where $k = 2\pi/\beta\lambda$ and $\omega = 2\pi f$, f being the rf frequency. The sinusoidal field distribution has a spatial period $\beta\lambda$ and temporal period $1/f$.

If the total energy of an ion is $W = \gamma mc^2$, the incremental energy gain is

$$\frac{dW_s}{dz} = qeE_z \cos\phi_s \tag{17}$$

where q is the number of charges e on the ion, and the energy W_s is that of a *synchronous* particle which travels along the traveling wave at a synchronous phase ϕ_s below the peak value of the accelerating field E_z. As will be seen, a negative ϕ_s produces a net longitudinal restoring force for particles around the synchronous particle.

The transit time variation from one accelerating gap to the next is related to the energy variation by

$$\frac{dt}{dz} = \frac{1}{v} = \frac{1}{c}\frac{\gamma}{(\gamma^2 - 1)^{1/2}}. \tag{18}$$

For any other particle of energy $W = W_s + \Delta W$, and noting that $d\phi = \omega dt$ and $d/d\gamma[\gamma(\gamma^2 - 1)^{-1/2}] = -1/\beta^3\gamma^3$, Eq. (18) becomes

$$\frac{d}{dz}(\phi - \phi_s) = -\frac{\omega}{m_0 c^3}\frac{\Delta W}{\beta_s^3 \gamma_s^3} \tag{19}$$

and Eq. (17) becomes

$$\frac{d\Delta W}{dz} = qeE_z(\cos\phi - \cos\phi_s). \tag{20}$$

These two equations may be combined into the second-order equation

$$\frac{d}{dz}\left(\beta_s^3\gamma_s^3\frac{d}{dz}(\phi - \phi_s)\right) = -\frac{2\pi}{\lambda}\frac{qeE}{mc^2}(\cos\phi - \cos\phi_s). \tag{21}$$

This nonlinear second-order differential equation describes the phase of a non-synchronous particle in the bunch. Particles describe paths in longitudinal phase-space around the particle with synchronous phase ϕ_s and energy W_s.

5.2 Small Longitudinal Oscillations

If the oscillation amplitude is small, we can linearize Eq. (21) around ϕ_s and W_s:

$$\frac{d^2}{dz^2}\Delta\phi = \frac{\omega}{c}\frac{1}{\beta_s^3\gamma_s^3 m_0c^2} qeET \sin\phi_s \, \Delta\phi. \tag{22}$$

The longitudinal oscillations have a wavelength

$$\lambda_\Omega = 2\pi \left(-\frac{\omega}{c}\frac{qeET}{m_0c^2}\frac{\sin\phi_s}{\beta^3\gamma^3} \right)^{-\frac{1}{2}}, \tag{23}$$

where T is the transit time factor (which will be derived in Section 6.5) and $E = 2AV/\beta\lambda$ is the peak longitudinal field in an RFQ with vane to vane voltage V and (unitless) accelerating parameter A, related to the depth of the vane scalloping by Eq. (32). For stability, $\phi_s < 0$. The bunch is on the rising slope of the rf waveform, and slower particles come later and get a larger kick, pushing them back into the bunch.

5.3 Nonlinear Longitudinal Oscillations

Equation (21) is nonlinear and the oscillation frequency is amplitude-dependent. Furthermore, above certain amplitudes, stability disappears and particles are lost longitudinally from the bunch. At this stability boundary in $\Delta\phi$–ΔW space, the oscillation frequency goes to zero, which defines the longitudinal *separatrix*, the dividing line in phase-space between longitudinal stability and instability.

The equation of motion can be found by multiplying Eq. (21) by $d\Delta\phi/dz$ and integrating:

$$\frac{1}{2}\beta_s^3\gamma_s^3 \left(\frac{d}{dz}\Delta\phi\right)^2 - \frac{qeE\omega}{m_0c^3}\left(\sin\phi - \phi\cos\phi_s + C\right) = 0, \tag{24}$$

where the constant C establishes a trajectory for a particular particle. In particular, if $C = (\sin\phi_s - \phi_s\cos\phi_s)$, then C defines the separatrix, where the trajectory is stationary.

The maximum energy excursion within the stability boundary occurs at $\phi = \phi_s$ and is given by

$$\Delta W = \pm 2\left[\frac{c}{\omega} qeEm_0c^2\beta_s^3\gamma_s^3(\phi_s\cos\phi_s - \sin\phi_s)\right]^{\frac{1}{2}}. \tag{25}$$

The maximum phase excursion ranges from $|\phi_s|$ to a point that must be determined numerically but is about $-2|\phi_s|$ for small values of ϕ_s. The length of the separatrix Φ_s is found by numerically solving

$$\tan\phi_s = \frac{\sin\Phi_s - \Phi_s}{1 - \cos\Phi_s}. \tag{26}$$

We have assumed that the parameters of the differential equation are stationary. In reality, the velocity β varies in each cell, along with ϕ_s and E. The effect in practical RFQs is to cause the separatrix to grow along the axis, which is optimized to capture nearly all the input unbunched beam. The *adiabatic buncher* will be described in a subsequent section.

6 RFQ Accelerator

In this section the field equations in the gap are derived. The geometry of the vane is defined, and the acceleration formalism derived in the last section is linked to the RFQ.

6.1 Vane Tip Modulations

We will derive the shape of the vanes to produce the proper transverse and longitudinal fields. The discussion will follow the formulation of Crandall [10].

Four parallel hyperbolic electrodes produce an electrostatic quadrupole field on the axis. A longitudinal field component is introduced by scalloping, or *modulating*, the tips of the vanes longitudinally, as shown in Figure 6. The scalloping

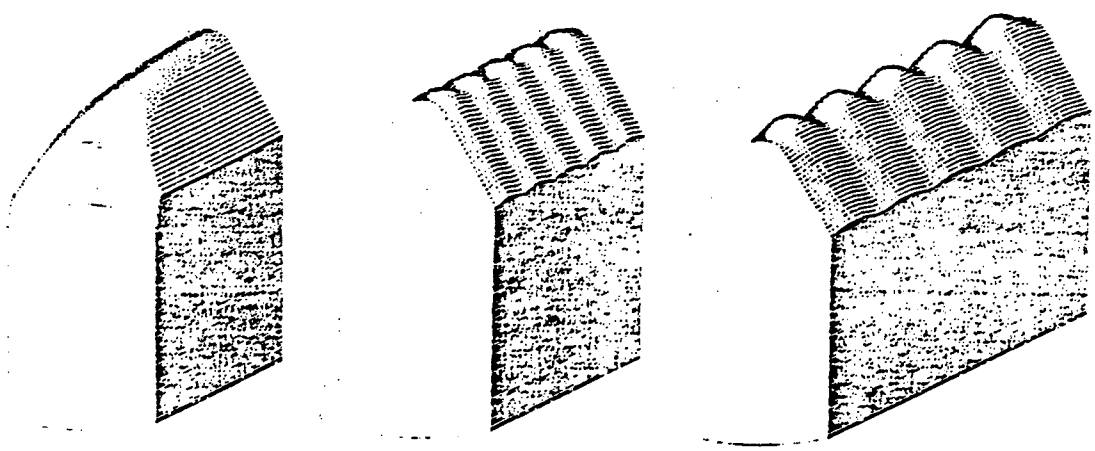

Figure 6: Scalloped Vane Tips

controls the strength of the longitudinal bunching and accelerating field while only slightly perturbing the strength of the transverse focusing field. The transverse focusing field is sustained along the entire length of the RFQ to maintain focus, and the longitudinal field is increased slowly along the axis to adiabatically bunch and capture the beam and then to accelerate it to full energy. In practice, most

of the length of an RFQ is devoted to the bunching process, with full acceleration occurring only near the exit end.

6.2 Potential Expansion

The potential in the region of the vane tips can be expanded as a Fourier-Bessel series:

$$U(r,\theta,z) = \frac{V}{2}\left[\sum_{m=1}^{\infty} A_{0m}\left(\frac{r}{r_0}\right)^{2m}\cos 2m\theta + \sum_{m=0}^{\infty}\sum_{n=1}^{\infty} A_{nm} I_{2m}(nkr)\cos 2m\theta \cos nkz\right]. \quad (27)$$

To a good approximation for most geometries, the first two leading terms characterize the potential near the axis (the two-term potential function):

$$U_{two-term}(r,\theta,z) = \frac{V}{2}\left[\left(\frac{r}{r_0}\right)^2 \cos 2\theta + AI_0(kr)\cos kz\right], \quad (28)$$

where we have set $A_{01} = 1$, and A_{10}, now simply called A, is the (unitless) two-term potential acceleration parameter. $L_c = \beta\lambda/2$ is the length of the unit cell, $k = \pi/L_c$, I_0 is the zero-order modified Bessel function, and r_0 is a normalizing radius, whose significance will be shown below.

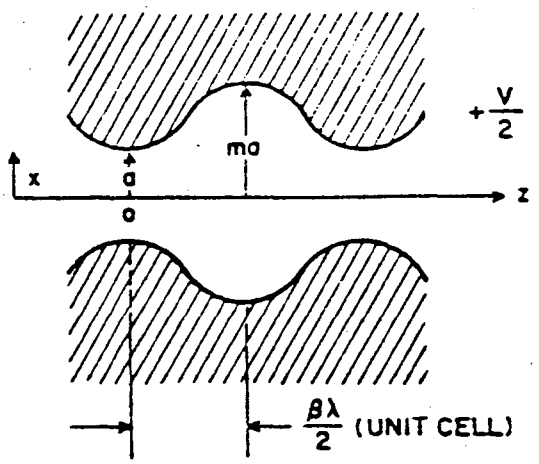

Figure 7: Vane Tip Longitudinal Profile

The scallops, or modulations of the vane surface, are shown in Figure 7. The distance from the axis to the edge of the quadrupole vane tip varies along the cell from a to ma, where $m \geq 1$ is the modulation depth. To establish a longitudinal field, the even and odd vanes have different radii from the axis. At longitudinal

position s, the even vanes are spaced a distance a from the axis and the odd vanes a distance ma. At position $s + \beta\lambda/2$, one accelerating cell away, the even-odd distances are reversed. This gives rise to an axial field dependent on m. For $m = 1$, the vanes are smooth, and $E_z = 0$. This is the same configuration as the Sloan-Lawrence accelerator shown in Figure 2.

6.3 Vane Tip Profile

The geometry of the surface of the vanes may be derived from the two-term potential function by applying the boundary conditions at the beginning and end of the unit cell $L_c = 0,\ \beta\lambda/2$.

$$\text{Even vanes}: \quad U(a,0,0) = U(ma,0,L_c) = \frac{V}{2}. \tag{29}$$

$$\text{Odd vanes}: \quad U(ma,\frac{\pi}{2},0) = U(ma,\frac{\pi}{2},L_c) = -\frac{V}{2}. \tag{30}$$

Equation (28) then gives

$$\left(\frac{a}{r_0}\right)^2 + AI_0(ka) = 1, \quad \left(\frac{ma}{r_0}\right)^2 - AI_0(mka) = 1, \tag{31}$$

or, when solved for A and r_0,

$$A = \frac{m^2-1}{m^2 I_0(ka) + I_0(mka)}, \tag{32}$$

$$\left(\frac{a}{r_0}\right)^2 = 1 - AI_0(ka). \tag{33}$$

We will define the focusing efficiency χ as

$$\chi \equiv 1 - AI_0(ka). \tag{34}$$

The normalizing radius r_0, the vane radius in the middle of the cell, is the point of quadrupole symmetry:

$$r_0 = a\chi^{-\frac{1}{2}}. \tag{35}$$

The modulation index $m \geq 1$ controls the longitudinal field strength E which is proportional to A as shown in Eq. (32). As A increases, the focusing efficiency, proportional to χ, decreases slightly. In practice, as the longitudinal field is ramped up along the structure, the focusing strength decreases slightly.

The cross-sectional shape of each vane is parabolic:

$$x^2 - y^2 = r^2 \cos 2\theta, \tag{36}$$

so Eq. (28) for $U = V/2$ on the vane tip yields

$$x^2 - y^2 = \frac{a^2}{\chi}\left\{1 - AI_0(kr)\cos kz\right\}. \tag{37}$$

For $\theta = 0$, we can trace a point along the $y = 0$ coordinate of the vane tip:

$$\frac{x^2}{a^2} = \frac{1 - A\, I_0(kx)\, \cos(kz)}{1 - A\, I_0(ka)}, \tag{38}$$

which can be solved numerically for $x(z)$ as a function of the cell parameters k, m, a, and A.

In the middle of the cell, at $z = \beta\lambda/4$, the radius $x = y = a\chi^{-1/2} = r_0$, which is the point of quadrupole symmetry. The focusing strength of a modulated structure is equivalent to that of an unmodulated vane with radius r_0.

6.4 Field Expansion

With the substitution $r_0 = a\chi^{-1/2}$, the field components derived from the potential function of Eq. (28) may be written in cylindrical coordinates:

$$\begin{aligned} E_r &= -\frac{\chi V}{a^2} r \cos 2\theta - \frac{kAV}{2} I_1(kr) \cos kz, \\ E_\theta &= \frac{\chi V}{a^2} r \sin 2\theta, \\ E_z &= \frac{kAV}{2} I_0(kr) \sin kz. \end{aligned} \tag{39}$$

where I_1 is the first-order modified Bessel function and a $\sin(\omega t + \phi_s)$ dependence has been assumed.

The first term in E_r and E_θ is the quadrupole focusing field expressed in cylindrical coordinates. The V/a^2 component is the electric field of a quadrupole with potentials $\pm V/2$ on the even (odd) vanes with aperture a. The vane tip modulations reduce the effectiveness of the focusing field by $\chi \leq 1$.

The second term of E_r is the gap defocusing term, which applies a defocusing radial impulse, roughly proportional to the displacement as $I_1(kr) \approx kr/2$. This term gives rise to the radial defocusing term Δ.

The E_z term is responsible for acceleration. The voltage across a unit cell $L_c = \beta\lambda/2$ on axis for $r = 0$ is just the integral

$$\Delta V_c = \int_0^{L_c} E_z\, dz = AV, \tag{40}$$

where $k = 2\pi/\beta\lambda = \pi/L_c$. The energy gained by a particle traversing a cell is not just AV, as the voltage $V = V_0 \sin(\omega t + \phi_s)$ varies as the particle crosses the cell, where the stable phase is ϕ_s. The energy gain ΔW of a particle crossing the cell is

$$\Delta W = qe \int_0^{L_c} E_z \sin kz\, dz = \frac{\pi}{4} AV \cos\phi_s. \tag{41}$$

6.5 Transit Time Factor

The transit time factor T is the ratio between the actual energy gain of a particle and the voltage across the cell:

$$\Delta W = qeAVT\cos\phi_s = qe\frac{\pi}{4}AV\cos\phi_s. \tag{42}$$

For RFQs with a sinusoidal longitudinal field distribution given by Eq. (39) the transit time factor T is just

$$T = \frac{\pi}{4}. \tag{43}$$

6.6 RF Defocusing

The form of the rf defocusing term Δ can be derived by comparing Eq. (10) with the force equation $\beta^2 mc^2 d^2x/ds^2 = qeE_r$ using the approximation $I_1(kr) \approx kr/2$:

$$\Delta = \frac{\pi^2}{2}\frac{qeV}{mc^2}\frac{A}{\beta^2}\sin\phi_s. \tag{44}$$

Normally $\phi_s < 0$ for longitudinal stability, setting $\Delta < 0$, which increases the divergence of a particle away from the axis. The rf defocusing strength goes as β^{-2} and is quite significant at the beginning of the accelerator. This is somewhat mitigated by a small longitudinal field, proportional to A at the beginning of the bunching and capture section.

6.7 Focusing Strength

As above, the focusing term B can be identified and is

$$B = \chi\frac{qeV}{mc^2}\frac{\lambda^2}{a^2}. \tag{45}$$

Note the important fact that the focusing strength is independent of the velocity of the ion: the focusing is uniform along the entire RFQ structure. This velocity independence is an important property of radio-frequency quadrupole focusing.

6.8 Peak Surface Field

The characteristics of an RFQ are strongly dependent on the design vane voltage. The transverse space-charge limit goes as the square of the vane voltage, for example. Generally, RFQs are designed with a vane voltage just short of the sparking limit.

The field on the surface of the vane with average displacement from the axis r_0 and voltage $\pm V/2$ (the vane-vane voltage is V), depends on the geometry of

the vane and the depth of the scallops. The peak field occurs where the vane tips have minimum separation. The peak surface field is given by

$$E_s = \frac{\kappa V}{r_0}, \tag{46}$$

where κ is the field enhancement factor. For round rods of radius equal to the nearest approach to the axis, $\kappa = 1.25$. For an unmodulated (smooth) vane with the shape given in Eq. (37), $\kappa = 1.38$. As the modulation factor m becomes greater than one, κ can reach values over 1.5.

The sparking limit is not a well defined quantity. It depends on the surface material, cleanliness, vacuum, and other (generally unknown) factors. However, an effort has been made to quantify the allowable peak surface field. Kilpatrick [11] measured the peak field between various surfaces under varying conditions and frequency and set a criterion of maximum field for a given frequency below which sparking is unlikely:

$$f = 1.643\ E^2\ e^{(-8.5/E)}, \tag{47}$$

where f is the frequency in MHz and E is the surface field in MV/m. Typical values of E for frequencies f of 50, 100, 200, and 425 MHz are 8.9, 11.4, 14.7, and 19.9 MV/m. These frequency-dependent field strengths are referred to as "one Kilpatrick."

The peak surface field in an RFQ, Eq. (46), is generally normalized to one Kilpatrick. Today, RFQs are being designed with peak surface fields in the range of 1.5 to 2.0 Kilpatrick. The field enhancement factor κ is geometry-dependent and requires a full three-dimensional electrostatic modelling calculation and can be estimated by using tables generated by Crandall [12]. Geometries with constant transverse radius have a smaller field enhancement κ than those with variable transverse radius of curvature. However, the variable transverse radius machines generally have a higher field quality with fewer significant multipole errors.

7 Bunching

One outstanding characteristic of the RFQ is its ability to bunch and capture nearly all the beam presented to it. This is accomplished by slowly increasing the longitudinal field along the axis of the structure, gently gathering the bunch up and preparing it for acceleration. This process requires many unit cells and is therefore not economical in conventional linacs with individual drift tubes. In RFQs, it is easy to include many short cells at the beginning of the structure with a small longitudinal field to provide adiabatic bunching.

8 Adiabatic Capture

The initial longitudinal beam entering the RFQ has little or no phase-space area. The dc beam is continuous, and within one accelerating bucket, the phase-spread is

uniform from $-\pi$ to π and the energy spread $\Delta W = 0$. As the beam propagates down the structure, the increasing longitudinal field, proportional to AV, first bunches the beam and then accelerates it.

The bunching process first takes place at a stable phase $\phi_s = -90°$, cf. Eq. (17), and the reference particle in the center of the bunch is not accelerated. The particles ahead of the reference particle are decelerated and fall back into the forming bunch; the particles behind are accelerated and catch up. The separatrix begins with no enclosed area, and as the bunch picks up energy spread, the separatrix height ΔW increases to contain the particle orbits.

Figure 8 shows the evolution of the longitudinal phase space during the adiabatic bunching process.

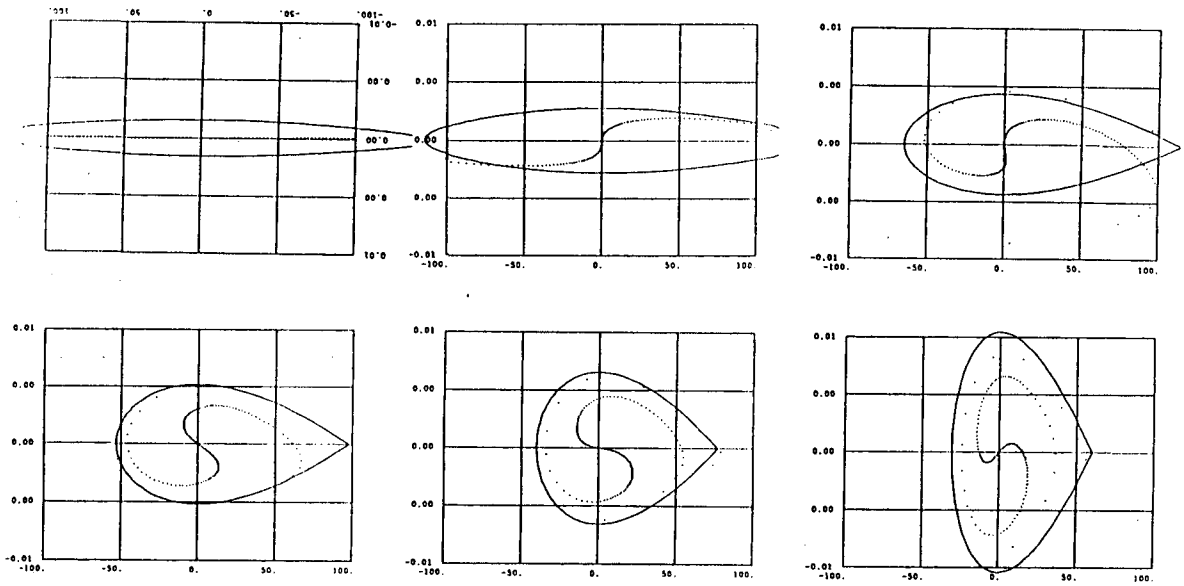

Figure 8: Adiabatically Bunching Longitudinal Phase-Space

8.1 Optimizing the Buncher

There is no unique best solution to the buncher in an RFQ. Many types have been tried, usually with good success. The requirements of accelerator length, output energy, and phase-spread and space-charge forces influence the choices. The method adopted by LANL [10] is to divide the RFQ into four sections:

Radial Matcher	Adiabatically matches dc input beam to strong transverse focusing structure.
Shaper	Starts the bunching process.

Gentle Buncher	Continues the bunching process until the beam is fully bunched.
Accelerator	Accelerates the beam at maximum acceleration rate to full energy.

The *shaper* is a short non-adiabatic section that is used to get the bunching process started.

The *gentle buncher* generally occupies most of the length of an RFQ, both bunching the beam and accelerating it up to an intermediate energy. The design of the buncher is adiabatic, but a true adiabatic buncher is infinitely long.

In the LANL method, based on the work by Kapchinskii and Teplyakov [1], the longitudinal oscillation frequency is given by

$$f_\Omega = \frac{\beta c}{\lambda_\Omega}, \tag{48}$$

where λ_Ω, the wavelength for small oscillations, given by Eq. (23), is kept constant, as is the bunch length

$$z_b = \frac{\beta \lambda \Phi_s}{2\pi}, \tag{49}$$

where Φ_s is the angular length of the separatrix, given by Eq. (26).

The design of the RFQ generally starts at the end of the buncher, where the beam has achieved its final desired value of ϕ_s. The above equations are used to calculate the cell parameters of the gentle buncher, working backwards, calculating the value of A, β, and ϕ_s for each cell. Since the adiabatic process starts with $\phi_s = -90°$, the gentle buncher calculated this way would be infinitely long. This description is stopped at a suitable point, such as $\phi_s = -88°$, and the short shaper section is inserted, which smoothly interpolates the cell parameters to $\phi_s = -90°$ and $A = 0$.

9 Injectors

The injector contains the ion source and the transport and focusing system that brings the beam to the RFQ entrance. The large focusing strength of the RFQ results in a beam of small diameter in the structure compared to the transverse size of the beam in the transport system. The last element of the transport system must rapidly compress the beam radially to match the acceptance of the RFQ, which typically requires a beam size somewhat smaller than 1 cm in diameter for proton RFQs.

9.1 Ion Sources

We will not cover ion source operation in this paper except to say that various RFQ designs are capable of accelerating a beam of high intensity and of low charge-

to-mass ratio q/A. Many types of ion sources have been successfully used with RFQs. The ion source emittance must be compatible with the RFQ acceptance, and the preacceleration potential must match the required RFQ injection energy.

The low injection energy requirement, compared to Alvarez linacs, considerably simplifies the design of the ion source platform. The low acceleration voltage required places the source near ground potential, usually under 100 kilovolts, simplifying access and reducing valuable building volume required for high-voltage apparatus. The modest accelerating voltage increases injector reliability and reduces operating manpower and costs.

9.2 Low Energy Beam Transport

The design of the low energy beam transport section (LEBT) is made somewhat more complex by the lower operating voltage and severe matching requirements into the RFQ. High current positive ion beams generally become fully neutralized by ionizing the background gas to provide neutralizing electrons. Negative ion beams form a three-component plasma, with high-mobility electrons and low-mobility positive gas ions together balancing the space-charge of the ion beam. This situation tends to be unstable, however, and the problem of H^- transport is not entirely solved. Effective neutralization requires a very quiet ion source plasma to suppress intensity oscillations that drive off the high mobility neutralizing electrons.

The strong transverse focusing strength of the RFQ requires a rapidly converging beam at the RFQ entrance. The last lens in the LEBT must focus the beam strongly into the RFQ radial matcher. Such strong lenses, where the transverse betatron function is rapidly changed, frequently suffer from spherical aberration and high sensitivity to mistuning. Lack of ability to achieve proper input match to the RFQ is one of the most-often-experienced problems in getting an RFQ-based linac to work properly.

10 Transverse Input Matching

The cross section of the beam from the ion source is time-independent. In the RFQ, the alternating gradient focusing causes the beam height and width to vary at the rf frequency. The stationary input beam envelope must be matched to the time varying envelope in the RFQ. To minimize the growth of transverse emittance due to the mismatch between the beam envelope parameters, an adiabatic *radial matcher* section is included.

The focusing parameter B is constant in the RFQ structure. In the radial matcher, the focusing strength is increased from zero, the value outside the struc-

ture, to B at the end of the radial matcher:

$$B(z) = \begin{cases} 0 & : \quad z < 0 \\ 0 \le f(z) \le B & : \quad 0 \le z \le L_{rm}. \\ B & : \quad \text{otherwise} \end{cases} \tag{50}$$

The functional form of $f(z)$ and the radial matcher length L_{rm} are not particularly critical. In practice, L_m is just a few cells long and $f(z)$ can rise from 0 to B linearly, or it can be smoothed with zero slope tangents at the ends. One form, due to Crandall [13], produces a very good match with negligible emittance increase:

$$B(z) = B\left[\frac{3}{4}\sin\left(\frac{\pi}{2}\frac{z}{L_{rm}}\right) - \frac{1}{4}\sin\left(\frac{3\pi}{2}\frac{z}{L_{rm}}\right)\right]. \tag{51}$$

The radial matcher is included in the vane geometry by varying the radius a. From the definition of B in Eq. (45), one sees that $a \propto B^{-1/2}$. The entrance end of the vane is machined in such a way that the radius begins with a large value at $z = 0$ and attains its final value of a at the end of the radial matcher.

11 RF Structures

So far we have considered the fields in the vicinity of the vane tips. We will now study the rest of the RFQ structure, which is responsible for putting the large rf voltage on the vane tips.

To develop large voltages at the tips of vanes at high frequencies requires resonant circuits. The two most frequently used cavity structures are the four-vane structure, based on a waveguide, and the four-rod structure, based on lumped inductances and capacitances. By driving a circuit at its resonant frequency, large rf voltages can be obtained.

11.1 Four-Vane RFQ

The four-vane RFQ structure shown in Figure 1 is based on exciting a circular waveguide in the TE120 mode, as shown in Figure 9. A section of the waveguide is enclosed between two metallic plates to form a resonant cavity. In the lowest longitudinal mode, the electric field has a $\sin 2\pi z/L$ dependence which satisfies the boundary condition of no transverse electric field at the endplates.

To generate an RFQ from the circular waveguide, four vanes are introduced which concentrate the displacement charges near the axis. The additional capacitive loading reduces the resonant frequency of the RFQ. In addition, a gap is left between the end of each vane and the endwall; the gap is tuned to the resonant frequency of the TE120 mode as shown in Figure 1. This alters the end boundary condition so that a constant vane voltage exists along the entire length of the cavity. The impedance of the tuned ends is equivalent to that of an infinitely long waveguide.

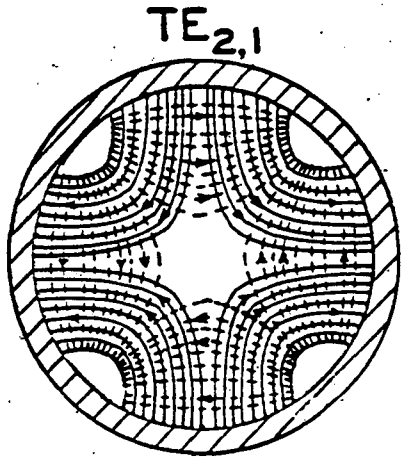

Figure 9: Circular Waveguide Excited by TE120 Mode

The magnetic field threads along each of the four quadrants around the ends in a baseball seam configuration. The magnetic field provides the rather weak coupling between the four quadrants. This results in a strong sensitivity to resonant frequency errors in the four quadrants.

The TE110 dipole mode in a circular waveguide has a somewhat lower resonant frequency than the TE120 quadrupole mode. However, when loaded by the vanes, the dipole and quadrupole modes can become degenerate and mix, producing a strong dipole field on the axis. This unwanted dipole field causes beam steering and poor RFQ operation. Remedies to this problem in four-vane RFQs are discussed in a following section.

11.2 Four-Rod RFQ

Another physical approach to the RFQ is the four-rod RFQ, as shown in Figure 10. Here, four rods are supported on inductive stubs, with the even and odd rods separately tied together and to their respective stubs. The stub inductance and the distributed capacitance of the rods form a lumped resonant circuit. The stored electric field energy is confined to the vicinity of the rods, and the magnetic field energy to the support stubs. The resonant frequency is not strongly influenced by the geometry of the vacuum chamber. As the even and odd rods are tied together, the unwanted dipole mode is not supported.

The four-rod RFQ is used primarily at lower frequencies for heavy-ion accelerators, and for intermediate-frequency (200-MHz) proton accelerators. It is a later development and is not yet as widely used as the four-vane structure.

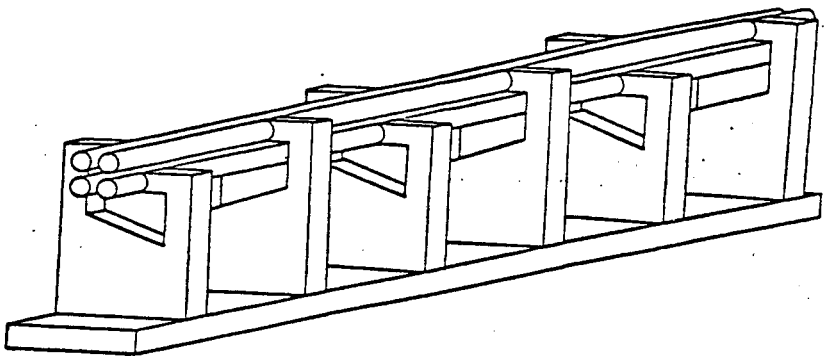

Figure 10: Four-Rod RFQ Structure

12 Mechanical Designs

All RFQs, no matter what the specific structure choice, must support an electric quadrupole field on axis with an appropriate longitudinal bunching and accelerating field. Both four-vane and four-rod structures contain vanes which are shaped to provide both focusing and accelerating fields. In this section we consider the vane tip shapes and the cavity structure that supports the vanes.

12.1 Vane Tip Shapes

The equation for the tip of the vane was derived in Section 6.3. Eqs. (28) and (34) can be written as

$$\left(\frac{r}{r_0}\right)^2 \cos 2\theta + AI_0(kr)\cos kz = \pm 1, \tag{52}$$

which defines the profile of the standard vane shape defined by the two-term potential function. At $\theta = 0$ or π the profile of $x(z)$ at $y = 0$ can be found by numerically solving this equation. The solution $x(z)$ will be called $\alpha(z)$. Similarly for $\theta = \pi/2$ or $3\pi/2$, $y(z)$ may be found. In the middle of each cell, at $z = L_c/2$ and $\cos kz = 0$, all four vanes are spaced r_0 from the axis, the point of quadrupolar symmetry.

If we rewrite Eq. (52) as

$$\frac{x^2 - y^2}{r_0^2} + AI_0(k\sqrt{x^2 + y^2})\cos kz = \pm 1, \tag{53}$$

then the transverse radii of curvature $\rho_\perp$ around the tip of the vane may be found by

$$\rho_t = \frac{(1 + x'^2)^{3/2}}{x''}, \tag{54}$$

where the differentiation is with respect to y. Along the tip of the horizontal vanes,

$$\rho_t(z) = \alpha(z)\left(\frac{P+Q}{P-Q}\right), \tag{55}$$

where

$$P = I_0(ka) + I_0(mka), \quad Q = \frac{ka^2}{2\alpha(z)}(m^2-1)I_1(k\alpha(z))\cos kz. \tag{56}$$

The longitudinal radius ρ_ℓ along the vane tip determines the maximum size of the cutter used to machine the surface. It may be found in a similar fashion to ρ_t by differentiating Eq. (53) with respect to z and finding the radius of curvature at the end of the cell where $z = L_c$, at which point $\alpha(z) = ma$. We find that

$$\rho_\ell(z = L_c) = \frac{2ma - Akr_0^2 I_1(mka)}{Ak^2 r_0^2 I_0(mka)}. \tag{57}$$

12.2 Vane Tip Machining

The determination of the minimum value of ρ_ℓ, which usually occurs near the end of the shaper, determines the maximum size of the tool that can be used to machine the vane. If ρ_ℓ is small, the the tool may be too small and may bend or break during the machining operation, or it may dull too quickly. This is a particularly difficult problem with RFQs for heavy ions or low injection energies. Also, the peak surface field enhancement tends to maximize around this area.

Vanes cut with this algorithm have a complex three-dimensional shape, as the transverse radius of curvature varies continuously along the vane. The vane must then be cut with, for example, a ball-end milling tool that traces the shape across the entire machined surface of the vane. This is a slow and exacting process.

An alternative cutting technique uses a form cutter which generates a constant-transverse-radius vane cross section. The transverse radius of curvature ρ_t is usually selected to be 70% to 100% of r_0. The vane tip cutting procedure proceeds much faster, as the entire vane tip surface can be cut in one pass, but the resulting geometry is a poorer approximation to the theoretical equipotential surface given by Eq. (28). In practice, the peak surface field enhancement is slightly lower, permitting higher vane voltages to be used, and the capacitance between the vane tips is more constant along the structure for varying modulation index m, but the undesirable harmonic content of the field is higher, possibly increasing the emittance of the beam.

12.3 Two-Term Potential Corrections

The two-term potential function is itself an approximation to the actual potential distribution given by the full Bessel-Fourier field expansion, Eq. (28). Normally, the RFQ is designed with a code such as PARMTEQ using the two-term potential,

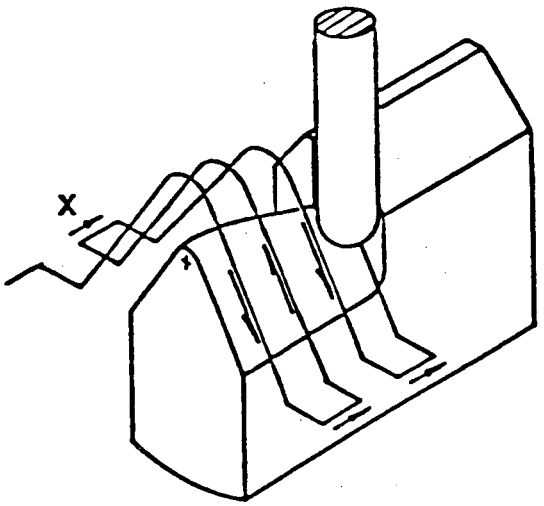

Figure 11: Tool path to cut variable curvature vane tip.

and then the geometry defined by a and m for each cell is slightly altered by adjusting these variables, based on a full three-dimensional electrostatic model of the actual vane tip surface, keeping r_0 constant. Several computer programs exist for doing this [12].

12.4 Four-Vane Structures

The most popular cavity structure for RFQs with resonant frequencies above 100 MHz is the four-vane structure shown in Figure 1. As shown in Section 11, the four-vane RFQ consists of a resonant waveguide section excited in the TE120 mode, loaded by vanes. The z-dependence of the transverse field in an empty TE120 cavity goes as $\sin \pi z/L_c$, but the inclusion of the vanes with the proper spacing from the endwalls flattens the field distribution.

The four quadrants form four separate resonant cavities, weakly coupled by the magnetic field that threads the four quadrants. Any misalignment destroys the quadrupole symmetry, resulting in nondegenerate resonant frequencies. This causes unequal rf excitation in each quadrant, generating dipole deflecting modes on axis. These modes interfere with the acceleration of the beam and cause loss and emittance increase.

The vane position tolerances required to suppress these unwanted dipole modes and other variations are beyond that which is considered practical in standard shop practice. The RFQ must be carefully tuned by moving the vanes after assembly and measuring the amplitude of the dipole mode mixing and of longitudinal variation of the field. Fortunately, methods have been discovered to stabilize the

structure; they will be discussed in Section 13.

12.5 Four-Rod Structures

The four-rod structure seems to be preferred for lower frequencies, where the TE120-resonant-cavity, four-vane structure would be very large. The four-rod structure avoids the dipole modes mentioned above, as the vanes are connected in pairs to resonant stubs connected to the vacuum cavity wall, as shown in Figure 10.

The four-rod structure is a little harder to design, as it does not lend itself to rf design programs such as SUPERFISH [14] or MAFIA [15], [16]. Usually, a set of rf models must be physically built to verify the resonant frequency and sensitivity to errors.

13 Structure Stabilization

A major drawback of the four-vane structure is its sensitivity to mechanical errors. Mismatch of the resonant frequencies of the four quadrants results in unequal excitation, exciting dipole modes, which interfere with the acceleration of the beam.

In addition, both the four-vane and four-rod designs are susceptible to errors in the longitudinal voltage distribution. Each type of structure can be modeled by a resonant transmission line whose local capacitance (resonant frequency) varies:

$$\frac{\partial^2}{\partial z^2}\left(\frac{\delta E_0}{E_0}\right) = \frac{8\pi^2}{\lambda_0^2}\left(\frac{\delta f}{f_0}\right), \tag{58}$$

where $\delta f/f_0$ is the local variation in resonant frequency, equivalent to one-half the variation in capacitance (or, equivalently, the spacing between the vane tips). The solution of Eq. (58), the relative field error, is proportional to $(L/\lambda_0)^2$, indicating that long, high-frequency structures are particularly sensitive to mechanical construction errors, which produce longitudinal field variation. Longitudinal field variation in each of the weakly coupled quadrants of the four-vane RFQ will produce a transverse dipole error with an axial strength dependence.

Several solutions to the unwanted TE110 dipole modes in the four-vane RFQ have been suggested. The first one to be widely used was to strap the alternate vane tips together with vane coupling rings [17]. This technique, shown in Figure 12, greatly reduces the sensitivity to assembly errors and reduces the RFQ tuning procedure to one of only establishing the proper longitudinal voltage distribution, usually by moving the endwalls.

Methods have been suggested to stabilize the longitudinal field distribution [18], [19]. They involve coupling resonant lines into the four-vane RFQ structure at selected longitudinal positions or introducing links at the endwalls which couple to the dipole modes. These methods are now starting to be applied to four-vane RFQs.

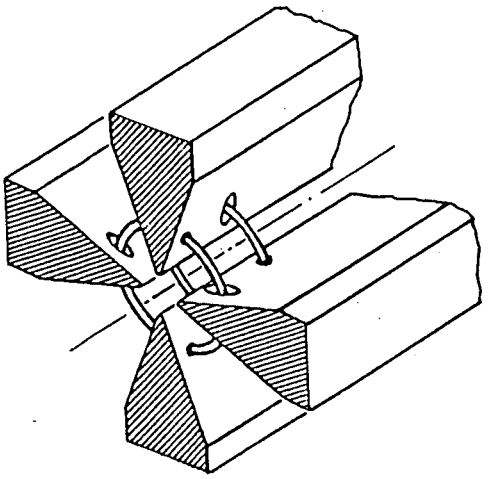

Figure 12: RFQ with Vane Coupling Rings

14 RF Considerations

In this section we consider several topics of interest to the rf power engineer.

14.1 Tuning and Vane Termination

The RFQ must be tuned to the proper frequency and the desirable field distribution and quality must be achieved. The cutoff frequency of the RFQ cavity is calculated with a code such as SUPERFISH [14], which models the RFQ as an infinitely long waveguide at cutoff frequency. In reality, the RFQ is a three-dimensional structure with end boundary conditions that can significantly perturb the resonant frequency, and with various other perturbations such as drive loops and mode stabilizers. Estimates must be made of these additional perturbations during the initial design process and appropriate frequency offsets introduced into the cavity design.

The vanes terminate a small distance from the endwall to establish the proper boundary conditions at the ends to create a constant potential along the entire length of the vane. The capacitance of the end of the vane to the endwall is resonated with the inductance of the stored magnetic field energy around the end of the vane to simulate the impedance of an infinitely long waveguide at the RFQ cutoff frequency. The design of the end of the vane is a complex computational problem [20] and is usually accomplished by the construction and measurements of cold (rf) test models.

The tuning process usually consists of making slight adjustments of the positions of the vanes once the preliminary mechanical alignment is finished, equalizing the excitation of the four quadrants. When vane coupling rings (VCRs) are fitted, this step can be eliminated. The end-to-end tilt is adjusted by varying the spac-

ing between the ends of the vanes and the endwalls, or by tuners fitted into the endwalls. The excitation can be measured by fitting several pickup probes to each quadrant, or by measuring the local electric and magnetic fields by perturbing them with a small object and measuring the resultant resonant frequency shift (bead perturbation measurements). The frequency shift varies as the volume of the perturber and the local field energy density.

14.2 Sparking Limit and Conditioning

The desirable parameters of the RFQ (acceptance, accelerating rate, current limit) increase rapidly with the vane voltage V, and therefore the surface field E_s. The voltage cannot be increased indefinitely, as at some point sparking will become very probable, as discussed in Section 6.8. Present RFQs operate to about a 2-Kilpatrick surface field and exhibit reasonable reliability if maintained with a good vacuum.

The rf amplifier should be capable of withstanding occasional sparks in the RFQ without damage. The impedance transformation from the RFQ to the plate circuit of the amplifier should be considered, as a spark in the RFQ results in a zero-impedance load at the end of the rf transmission line. To reduce the rf plate voltage during the spark, a transmission line length of a multiple of a half wavelength may be desirable.

When an RFQ is first operated, it will spark and multipactor at lower fields. (Multipactoring is an ion resonance phenomenon common with unclean surfaces where both rf electric and magnetic fields are present). The rf amplifier must be capable of tolerating considerable sparking during the conditioning process, and must be capable of driving the RFQ very hard to break through the many multipactor levels. Gas bursts will accompany the conditioning process, which must be throttled back to accommodate the vacuum pumps.

14.3 Cooling, Vane End Power

The rf power dissipation can easily be calculated with codes such as SUPERFISH. The power dissipation at the end of the vanes can be considerably higher, however, as there is usually an enhancement of the rf magnetic field. This is more difficult to estimate, but can be significant for high-duty-factor machines.

For low-duty-factor operation, the total power dissipated in the RFQ may be so low as not to require cooling at all, as long as the tuners can keep the RFQ on the desired frequency. High-duty-factor machines are a triumph of providing cooling passages everywhere and dealing with melted components.

14.4 Tuners

RFQs are tuned to frequency by inserting objects in the regions of high magnetic field. Excluding a volume of magnetic field raises the resonant frequency.

If the tuning is local and strong, the field distribution along the RFQ may be significantly perturbed. If the quadrants are not strongly coupled with VCRs or equivalent mode stabilizers, the tuners must be symmetrically distributed in all four quadrants.

The tuners usually take the form of paddles or rings whose area perpendicular to the direction of the magnetic field can be changed by rotation, or by pistons that can be inserted into the RFQ volume. RF and vacuum seals must be provided that are compatible with the rf levels present without burnup.

14.5 VCR Perturbations

If vane coupling rings are provided to strongly couple the quadrants, the frequency perturbation due to the increased capacitance between the vane tips must be taken into account. In addition, the lowered local resonant frequency in the vicinity of each set of coupling rings *increases* the electric field at that point (the washline effect).

The VCR frequency perturbation is not easily estimated but has been measured with rf models. The electric field enhancement can be calculated from the frequency perturbation.

14.6 Drive Loop Compensation

The drive loop is usually introduced through a hole in the side of the cavity which can add to the volume of magnetic field energy, lowering the local resonant frequency of the quadrant. Dummy holes can be introduced in the other quadrants at that longitudinal position, or the center conductor of the drive loop itself can contain a perturbing volume to compensate the frequency perturbation [21].

14.7 Vacuum Ports

The RFQ is pumped through holes introduced into the outer walls of the cavity in regions of high rf magnetic field. The field penetrates the holes, reducing the resonant frequency. In addition, the current in the walls runs circumferentially, and the vacuum ports should be designed to minimally perturb the current paths.

If the holes are too large or thin in radial extent, rf power can leak from the cavity and be radiated into the vacuum system.

14.8 Beam Loading

Beam loading presents a complex load (purely resistive if $\phi_s = 0$) unevenly distributed along the cavity, mostly in the acceleration section. If the RFQ transfers a significant fraction of the input power to the beam, loading compensation in the form of longitudinal compensators or distribution of drive ports may need to be provided.

15 Space-Charge Effects

In this section we will consider the effects of beam space-charge on the transverse and longitudinal dynamics of the acceleration process and how to optimize the design in the presence of significant space-charge [22].

15.1 Transverse Space-Charge

Space-charge in the bunch generates a repulsive force on the particles at the periphery of the bunch. The focusing force is partially canceled, reducing the effective tune of the focusing structure. The beam size increases and may completely fill the aperture. The space-charge fields are nonlinear, which may increase the beam emittance.

We will follow the discussion by Wangler [7] to calculate the maximum current that can be accelerated in an RFQ. The transverse and longitudinal limits are inversely dependent on the transverse focusing strength: as the bunch is more tightly focused transversely, the higher linear charge density increases the longitudinally defocusing space-charge force, reducing the peak current that can be accelerated. The analogous argument applies to longitudinal focusing. The choice of RFQ parameters requires balancing many interrelated items.

The bunch is modeled by a symmetric ellipsoid of uniform charge density ρ of radius r and half-length b. The fields within the ellipsoid are

$$\begin{aligned} E_x &= \frac{\rho x[1-f(p)]}{2\epsilon_0}, \\ E_y &= \frac{\rho y[1-f(p)]}{2\epsilon_0}, \\ E_z &= \frac{\rho z f(p)}{\epsilon_0}, \end{aligned} \tag{59}$$

where the charge density ρ is related to the average current I in the beam by

$$\rho = \frac{3I\lambda}{4\pi r^2 bc}. \tag{60}$$

The uniform charge density within the bunch envelope is highly idealized and is the only one that produces linear space-charge forces (the Kapchinskii-Vladimirskii [23] distribution). A more realistic model but one that cannot be solved analytically introduces a non-uniform distribution which produces an emittance increase due to the non-linear nature of the space-charge field. The form factor $f(p)$ depends

on the axis ratio $p = b/r$ and is given by

$$f(p) = \begin{cases} \dfrac{1}{1-p^2} - \dfrac{p}{(1-p^2)^{3/2}} \cos^{-1} p & : \ p < 1, \\ \dfrac{1}{3} & : \ p = 1, \\ \dfrac{p \cosh^{-1} p}{(p^2-1)^{3/2}} - \dfrac{1}{p^2-1} & : \ p > 1, \end{cases} \tag{61}$$

which can be approximated by $f(p) \approx r/3b$ for $0.8 < p < 5$.

Adding the defocusing due to space-charge, Eq. (10), to the transverse equation of motion, we obtain

$$\beta^2 \lambda^2 \frac{d^2x}{dz^2} = (B_0 \sin kz + \Delta_{rf} + \Delta_{sc})x, \tag{62}$$

where

$$\Delta_{sc} = -\frac{3Z_0}{8\pi} \frac{qeI\lambda^3}{mc^2 r^2 b}[1 - f(p)], \tag{63}$$

and $Z_0 = 1/\epsilon_0 c = 377\Omega$. For notation consistent with the literature, we note that

$$\theta_0^2 \equiv B = \frac{qeV\lambda^2\chi}{mc^2a^2}, \tag{64}$$

The unperturbed tune σ_0 and perturbed tune σ are

$$\sigma_0^2 = \frac{\theta_0^4}{8\pi^2} + \Delta_{rf} \tag{65}$$

and

$$\sigma^2 = \frac{\theta_0^4}{8\pi^2} + \Delta_{rf} + \Delta_{sc}. \tag{66}$$

The beam size x depends on the betatron amplitude $\beta(z)$ and emittance ϵ:

$$x(z) = \sqrt{\epsilon\beta(z)}. \tag{67}$$

We will define the transverse space-charge parameter μ_t as

$$\sigma^2 = \sigma_0^2(1 - \mu_t), \tag{68}$$

so we see that μ_t is the ratio of space-charge force to restoring force:

$$\mu_t = -\frac{\Delta_{sc}}{\sigma_0^2}. \tag{69}$$

We can solve Eq. (63) and (69) for the current I corresponding to a given value of the space-charge parameter μ_t:

$$I_t = \frac{8\pi}{3Z_0}\mu_t \frac{mc^2}{qe}\frac{r^2 b\sigma_0^2}{\lambda^3[1-f(p)]}. \tag{70}$$

We can cast this into a more useful form. The bunch half-length b is approximately related to the stable ϕ_s phase by $b = \beta\lambda|\phi_s|/2\pi$. If the beam is allowed to fill the aperture a, then the average beam envelope radius is $r^2 = a^2/\Psi$, where the flutter factor Ψ is the ratio of maximum to minimum envelope size described in Section 4.3.

With $\sigma_0^2 = B^2/8\pi^2$, the current limit can be expressed as

$$I_t = \frac{4}{3}\frac{\mu_t}{Z_0}\frac{mc^2}{qe}\frac{\beta|\phi_s|B^2}{8\pi^2\Psi[1-f(p)]}\left(\frac{a}{\lambda}\right)^2. \tag{71}$$

For periodic focusing systems, the envelope size is minimized if the zero-space-charge phase advance per focusing period is about 90°: $\sigma_0 \approx \pi/2$, or $B \approx \pi^2\sqrt{2}$.

Equation (71) represents the maximum current for transverse stability with the beam contained within the aperture if the focusing strength can be adjusted to produce the required zero-current phase advance $\sigma_0 = \pi/2$ per focusing period. If the voltage V between the vanes is limited by sparking, then B must be reduced, along with the focusing phase advance σ_0. Using Eq. (65) and the definition of B, we find

$$I_t = \frac{\mu_t}{6\pi^2 Z_0}\frac{qe}{mc^2}\frac{\beta|\phi_s|(\lambda\chi)^2}{\Psi[1-f(p)]}\left(\frac{V}{a}\right)^2\left[\frac{B^2+8\pi^2\Delta_{rf}}{B^2}\right]. \tag{72}$$

We see that the transverse current goes as $\beta\lambda^2V^2$. Experience shows that the maximum practical tune depression which still allows stable beam transport is

$$\frac{\sigma}{\sigma_0} \approx 0.4, \tag{73}$$

which gives

$$\mu_t \approx 0.84 \tag{74}$$

in Eq. (72).

15.2 Longitudinal Space-Charge

The longitudinal space-charge limit can be determined in a similar fashion. Longitudinal space-charge reduces the longitudinal stability by reducing the effective focusing forces at the ends of the bunch. The linearized longitudinal equation of motion, Eq. (22), can be expressed as

$$\frac{d^2}{dz^2}\Delta\phi = \frac{2\pi}{\lambda}\frac{1}{\beta_s^3\gamma_s^3 m_0c^2}qeET\sin\phi_s\,\Delta\phi = \frac{\sigma_\ell^2}{\beta^2\lambda^2}\Delta\phi, \tag{75}$$

where we have introduced the longitudinal space-charge by the substitution

$$\sigma_\ell^2 \rightarrow \sigma_{\ell,0}^2 + \Delta_{sc,\ell}. \tag{76}$$

The space-charge term can be derived from the longitudinal space charge field E_z as

$$\frac{\Delta_{sc,\ell}}{\beta^2\lambda^2} = \frac{qe}{mc^2\beta^2}\frac{3Z_0}{4\pi}\frac{I\lambda f(p)}{r^2 b}. \tag{77}$$

The longitudinal space-charge parameter is defined as

$$\mu_\ell = -\frac{\Delta_{sc,\ell}}{\sigma_{\ell,0}^2}. \tag{78}$$

Substituting and solving for the longitudinal current limit corresponding to a given value of longitudinal space-charge parameter μ_ℓ, we obtain

$$I_\ell = \frac{4\pi^3}{3Z_0}\mu_\ell\frac{r^2 b}{\beta^2\lambda^3 f(p)}\sin\phi_s. \tag{79}$$

Again, substituting for r^2, b, and $f = r/3b$ as before, the longitudinal current limit for an RFQ is

$$I_\ell = \frac{\pi}{Z_0}\mu_\ell\frac{a}{\Psi^{1/2}}\frac{\phi_s^2}{\lambda}AV|\sin\phi_s|, \tag{80}$$

where, as before, we can set $\mu_\ell = 0.84$. Here, we see that the longitudinal space-charge limit goes as V/λ.

15.3 Optimizing the Overall Design

The design of an RFQ involves compromises between transverse and longitudinal stability, between acceptance and power demand, and between many other factors.

The beam at the entrance of the RFQ is unbunched and large but converging transversely. Longitudinal space-charge is not a factor until the beam becomes fully bunched at the end of the gentle buncher section. After the radial matcher, the focusing strength is usually constant all the way to the end of the machine. In four-vane RFQs, to keep the resonant frequency of the structure constant along the entire length, r_0 is usually kept constant, and the vane tip voltage V is also usually kept constant.

The beam achieves full bunching at the end of the gentle buncher. Generally, the energy is still low at this point so the space-charge forces are the most significant. It is at this point that the design of the RFQ is optimized in terms of its response to space-charge. At a lower energy, the bunch density is lower, as the adiabatic bunching process is yet incomplete, and at higher energy the velocity dependence of the transverse current limit reduces the significance of the space charge forces.

We see from Eq. (72) and (80) that

$$I_t \propto \beta\lambda^2 \frac{V^2}{a^2}\phi_s \tag{81}$$

and

$$I_\ell \propto \frac{V}{\lambda}\phi_s^2 a. \tag{82}$$

This indicates, for example, that a low frequency (large-λ) machine is preferred for a large transverse current limit, but a high-frequency machine would have a higher longitudinal current limit. Other machine parameters a, V, and ϕ_s all indicate compromises are required to optimize the structure.

Fortunately, computer programs (CURLI [24], for example) are available that help optimize the RFQ parameters for given sets of constraints. Even then, the design process requires some experience, as the parameters of an RFQ are strongly interactive and some effects are counterintuitive. The designs of the shaper and gentle buncher sections have a strong influence on the bunching process, the longitudinal emittance of the emerging beam, and the fraction of the input beam that is captured and accelerated to full energy. There is no simple recipe to assure an optimized design. Some of the computer codes that are frequently used are described in the next section.

16 Beam Dynamics Codes

The design of the RFQ is divided into two parts: selecting the cell structure to satisfy the particular user beam requirements of energy, acceptance, output energy spread, and the like; and designing the actual rf structure to resonate at the required frequency, establishing the rf power requirement, analyzing the distribution of cavity wall power dissipation, and analyzing the sensitivity to mechanical errors.

The beam dynamics part of the design is the result of an interplay and compromise between conflicting constraints of phase-space acceptance, susceptibility to sparking between the vane tips, power requirement, and the like. The success of the design depends as much on the intuition of the designer as on the quality of construction.

Fortunately, RFQ designers have a standard set of computer codes to use to design the cell sequence and simulate the acceleration of particles. The code PARMTEQ [24] written at LANL (and never really documented) is used to track particles through a simulated machine. The value of using a standard code is obvious: designs can be compared between laboratories, and new design ideas can be easily shared.

PARMTEQ is not used to actually design the machine: it accepts design data from other codes (not so universally shared), tracks particles, and predicts the output beam parameters. The program accepts the design data (the variables

a, m, ϕ_s, and V specified for each cell), and generates a representation for each cell, by which it can calculate all the geometric cell parameters and the field components E_r, E_θ, and E_z.

An ensemble of particles representing the input beam with the desired phase-space distribution is generated and tracked through each RFQ cell. The cell is subdivided longitudinally and the integrals of motion are replaced by finite steps. Particles that exceed the aperture limit are lost. At the end of the machine, the statistics of the exit beam are calculated. Graphical representations of the phase-space planes and the particle trajectories are produced.

The actual design of the machine is accomplished with driver programs such as CURLI, which models the space-charge [24] behavior of the bunch in typical cells of the RFQ, and RFQUIK, which is used to design the gentle buncher and shaper sections. The design process is an iterative procedure, adjusting compromises between the desired beam transmission and output phase-space, and the machine length, power requirement, ease of production, and other considerations. The RFQ is a subtle device and good design requires some experience and artistry.

17 Cavity Design Codes

The RFQ consists of a resonant cavity which can be modeled by many existing two- and three-dimensional electromagnetic Poisson solver codes.

17.1 Four-Vane Structures

The four-vane RFQ is usually approximated in cross section by an infinitely long waveguide. The cutoff frequency and parameter sensitivity are determined with a two-dimensional code such as SUPERFISH [14]. As the RFQ has fourfold symmetry, only one quadrant is modeled. Dipole deflecting modes are modeled by including two adjacent quadrants. Figure 13 shows the predicted field configuration for a typical four-vane RFQ.

The ends of the RFQ are tuned to the cutoff frequency of the waveguide. Traditionally, this has been a "cut and try" technique, frequently with physical cavity models, but recently the ends have been modeled with three-dimensional codes such as MAFIA [20].

17.2 Four-Rod Structures

The four-rod structure is more difficult to model with mesh codes, as it has less symmetry, requiring full detailed three-dimensional modeling beyond the capabilities of available codes. Four-rod structures are generally physically modeled with small "cold models" and their parameters can also be estimated based on lumped-circuit analysis.

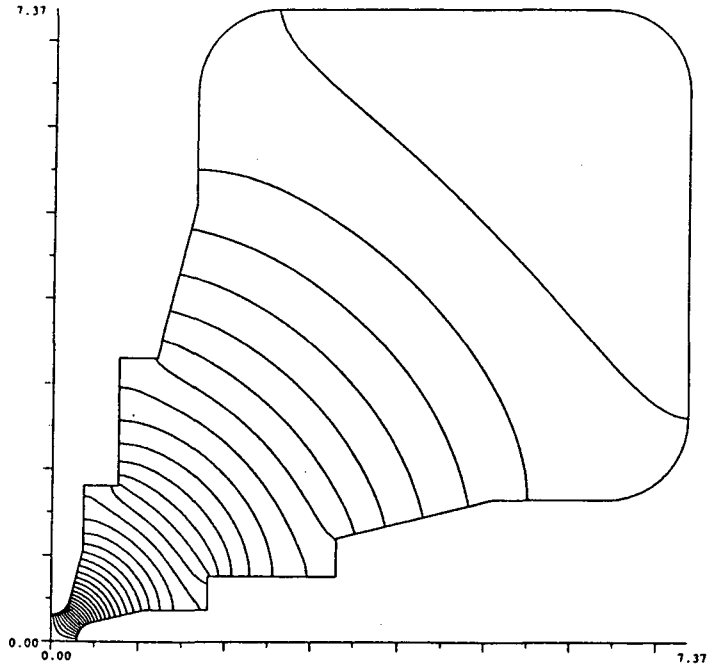

Figure 13: Field Lines Calculated by SUPERFISH

The capacitance between the rods and the inductance of the stub supports can be evaluated fairly accurately with geometric analogues, giving a good estimate of the resonant frequency.

18 Some Real Machines

In this section we will look at several RFQs that have been built and operated. Many interesting engineering ideas have emerged from the several laboratories now engaged in RFQ design.

18.1 LANL RFQs

Two of the low-duty-factor RFQs built at LANL are described here: the AT-2 [25] machine, built as a test bed for neutral particle beam weapons simulation and the BEAR (beam experiment aboard a rocket) RFQ that was the first ion accelerator of significant energy to be launched into space [26].

The AT-2 machine was designed and built around 1980. It is now considered to be an older design, but it pioneered many ideas that were first being developed at LANL such as the rf power manifold, which surrounded the RFQ cavity and fed it through several coupling slots. This is a very long RFQ, and exhibited a strong

sensitivity to vane position error until vane coupling rings were later included. This RFQ ran for almost 10 years, delivering beams of very high quality.

Table 1: LANL Four-Vane RFQs

RFQ	AT-2 (1982)	BEAR	
Ion	H^-	H^-	
Freq	425	425	MHz
T_{in}	100	30	keV
T_{out}	2072	1000	keV
Length	289	100	cm
r_0	0.394	0.171	cm
No. Cells	356	154	
Acceptance	0.23π		cm-mrad
RF Power		70	kW
Vane Voltage	111	44	kV
E_s	41.4	37.3	MV/m
	2.06	1.85	Kilpatrick
Focusing B	3.8	9	

The BEAR RFQ is a compact and lightweight RFQ used to test propagation of a partially neutralized H^- beam in the exosphere. It was built of four nearly identical sections (except for the vane tip modulations) electroformed together at joints running lengthwise along the structure for structural rigidity. It survived the rigors of launch and performed flawlessly in a space environment. Figure 14 shows the general construction of this accelerator. Table 1 lists important parameters of these two RFQs.

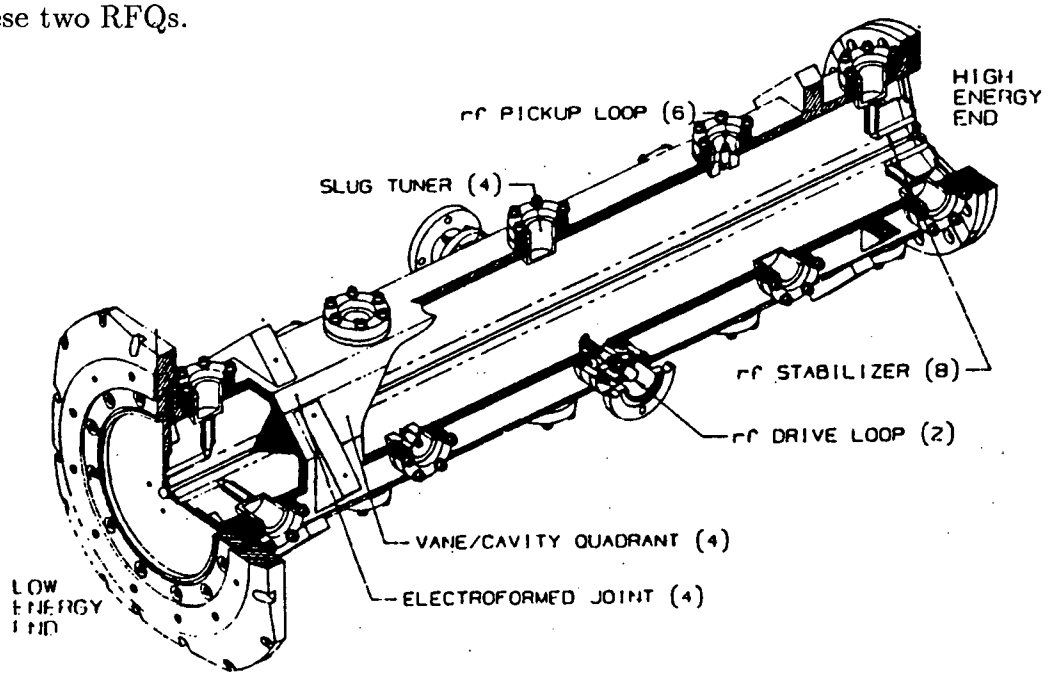

Figure 14: LANL/Grumman BEAR RFQ

The AT-2 RFQ is of conventional design with a very short shaper section and a relatively long gentle buncher section compressing the beam longitudinally. The BEAR RFQ included a relatively long shaper and shorter gentle buncher, which reduced the overall length of the RFQ but made the output energy spread more dependent on the input current. Interestingly, at lower input current, the longitudinal pulse compression is not limited by the presence of longitudinal space-charge, and the overcompression causes an increase in the output energy spread.

18.2 LBL Four-Vane RFQs

LBL has designed and built three RFQs of almost identical mechanical design for the acceleration of silicon [27], [28], oxygen [29], and protons [30], [31]. These machines are of conventional 4-vane design and are the first machines to use vane coupling rings (VCRs) [17] to control the unwanted dipole modes due to vane misalignment errors.

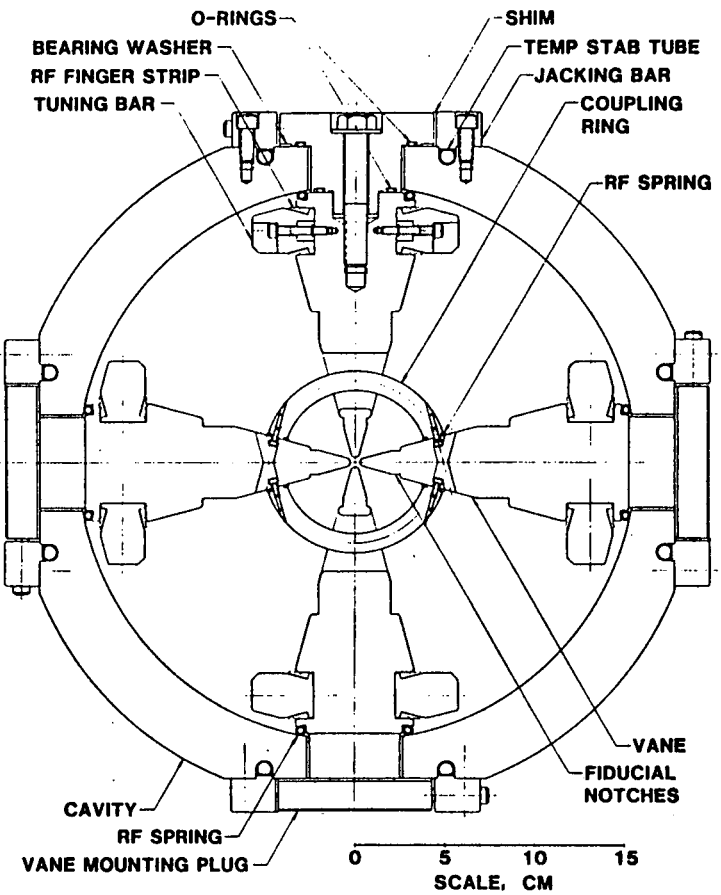

Figure 15: LBL Four-Vane RFQ Arrangement

Figure 15 shows the mechanical arrangement of the LBL 4-vane RFQ [32]. Each vane is separately mounted in a cylindrical cavity by a series of mounting plugs that penetrate the thickness of the cavity and rest on precision flat fiducial surfaces on the outside diameter. The relative locations of the fiducial surfaces

can be accurately determined with standard shop practice. The mounting plugs engage precision surfaces on the back edges of the four vanes. The radial and lateral positions of the vanes are independently adjustable and are determined by shims. Table 2 lists the important parameters of these three machines.

Table 2: LBL Four-Vane RFQs

RFQ	LBL	CERN	BNL	LBL2	
Ion	Si^{+4}	O^{+3}	p^+	p^+	
Freq	199.3	202.56	201.25	410	MHz
q/A	1/7	3/8	1	1	
T_{in}	8.4	5.63	35	40	keV/n
T_{out}	200	139.4	753	800	keV/n
Length	224	85.8	161.9	101.7	cm
r_0	.254	.211	.418	.303	cm
No. Cells	346	169	146	160	
Cavity ID	15.583				cm
Acceptance	0.05π	0.09π		0.05π	cm-mrad
RF Power	150	21	100	160	kW
Vane Voltage	51	35.6	67.2	72	kV
E_s	27	25.9		37	MV/m
	1.85	1.76	1.47	1.9	Kilpatrick
Focusing B	2.7	7→4	9.1		

A fourth machine, a small 800-keV proton device, was also built at LBL to test a construction technique applicable to mass production. The vanes are part of the cavity itself, which fits together at fiducial surfaces, allowing reproducible alignment of the entire machine to better than 25 μm without precision tooling [33]. Figure 16 shows a cross section of this machine.

18.3 High-Duty-Factor RFQs

RFQs are capable of 100% duty factor operation. An earlier RFQ, the Fusion Materials Irradiation Test (FMIT) [34] machine, was built at LANL in the early 1980s and operated with a $q/A = 1/2$ ion (H^-). This RFQ would have been the front end of a 100-mA, 35-MeV deuteron linac in an arrangement providing intense neutrons for testing candidate reactor-wall lining materials for inertial fusion. The rest of the linac was never built, but experience was gained in operating an RFQ at nearly 100% duty factor.

The RFQ-1 device at Chalk River National Laboratory (CRNL) started operating in 1988 [35], [36] and has been used to investigate many of the problems of high average power. This machine is part of a discontinued program to provide a high-energy, continuous source of protons. Figures 17 and 18 show these two

RFQs and Table 3 lists some important parameters.

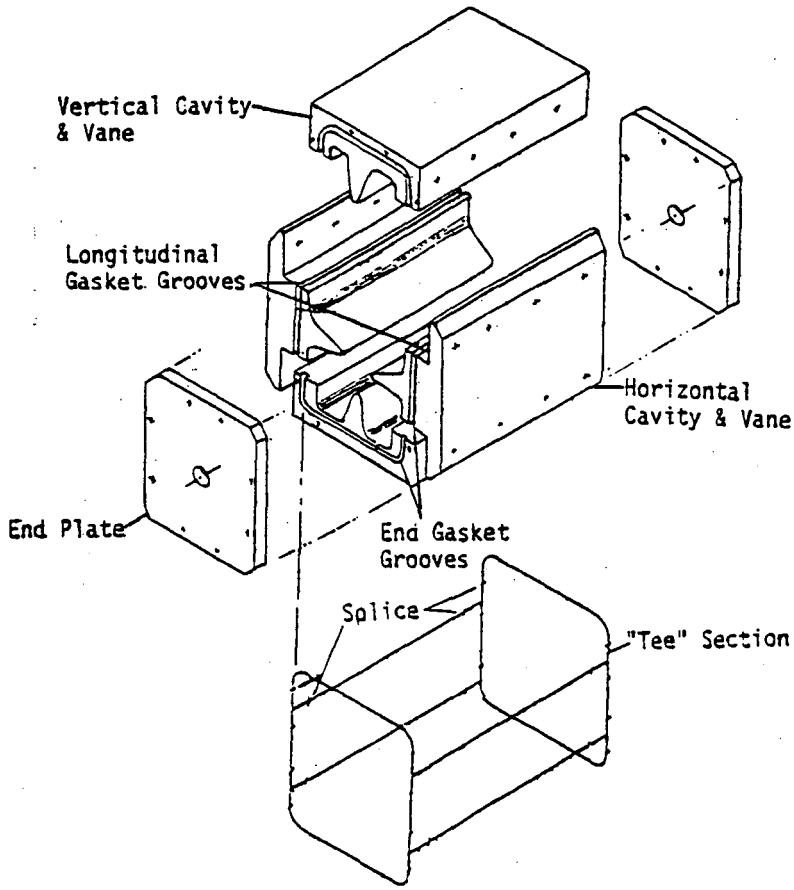

Figure 16: LBL Integrally Formed RFQ

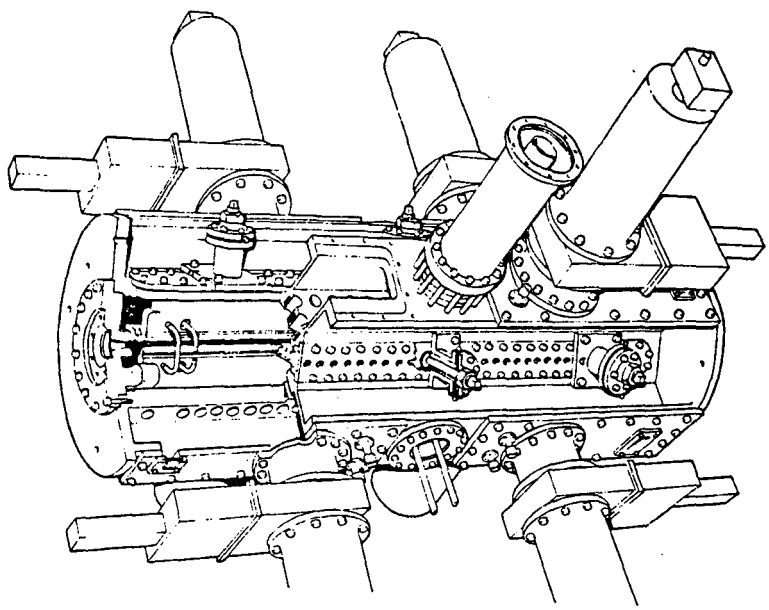

Figure 17: CRNL RFQ-1

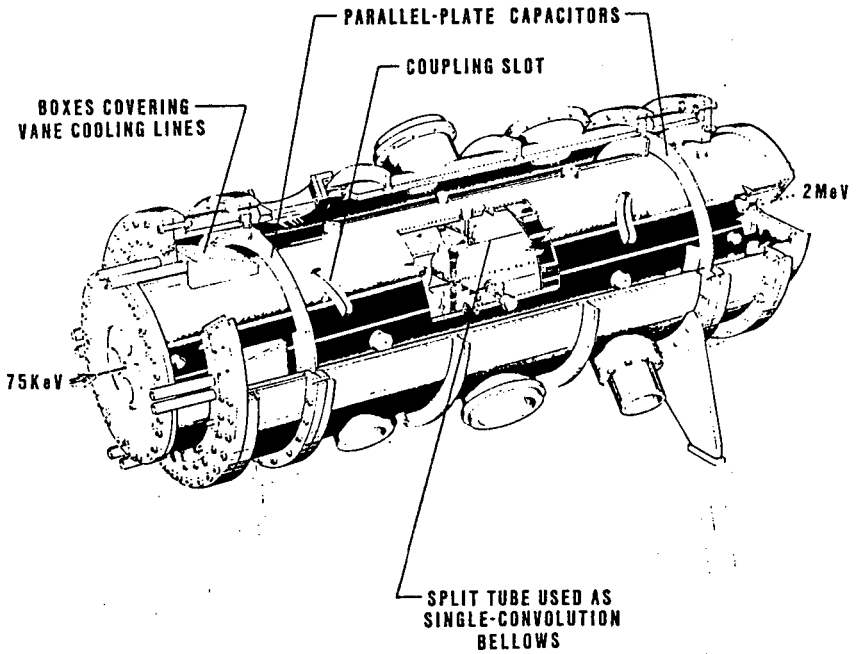

Figure 18: FMIT RFQ

Table 3: High-Duty-Factor RFQs

RFQ	FMIT	RFQ-1	
Ion	D^+	proton	
Freq	80	267	MHz
T_{in}	75	50	keV
T_{out}	2000	600	keV
Length	408	150	cm
r_0		0.403	cm
No. Cells		181	
Cavity ID	85.9		cm
RF Power	491	130	kW
Vane Voltage	183	78	kV
E_s	17.5	25	MV/m
	1.68	1.5	Kilpatrick
Focusing B	6.9	6.2	
Max Current	205	100	ma

18.4 Four-Rod RFQs

Many four-rod RFQs have been built and operated (see Table 4), with the center of activity at the University of Frankfurt. We present here one Frankfurt RFQ to be used at GSI in the heavy ion injector capable of uranium acceleration [37], and

a prototype front-end RFQ built at the Institute for Theoretical and Experimental Physics (ITEP) in Moscow for the acceleration of doubly charged bismuth for an inertial confinement fusion driver [38]. Figure 10 shows the arrangement of a four-rod RFQ built at Frankfurt.

Table 4: Four-Rod RFQs

RFQ	U28	ITEP	
Ion	U^{+28}	Bi^{+2}	
Freq	108.5	6.19	MHz
q/A	0.117	0.01	
T_{in}	2.5	1	keV/n
T_{out}	300	50	keV/n
Length	290	16400	cm
r_0	0.42	2.2	cm
Acceptance	0.08π	0.25π	cm-mrad
RF Power	100	2000	kW
Vane Voltage	80	190	kV
E_s		12.2	MV/m
		2.5	Kilpatrick
Focusing B	4.3	10	

18.5 Split Coaxial Resonator RFQs

For acceleration of low-charge-state heavy ions, a low frequency structure is called for. An alternative to the four-rod structure is the split coaxial resonator structure, pioneered at GSI and at the Institute for Nuclear Studies at the University of Tokyo [39].

Table 5: INS Split Coaxial Resonator RFQ Parameters

RFQ	INS	
Freq	50	MHz
q/A	1/7	
T_{in}	2	keV/n
T_{out}	59.6	keV/n
Length	205.2	cm
No. Cells	168	
r_0	0.541	cm
Acceptance	0.03π	cm-mrad
RF Power	13.2	kW
Vane Voltage	20.3	kV
Focusing B	3.8	

As Figure 19 shows, the even vanes are connected to one end of a pillbox cavity excited in the TM mode and the odd vanes to the other end wall, so an

e.m.f. exists between the endwalls and therefore between the vanes themselves. A potential is set up between the even and odd vanes, producing a quadrupole field on axis. The very large capacitance between the vanes loads the cavity heavily, lowering the frequency.

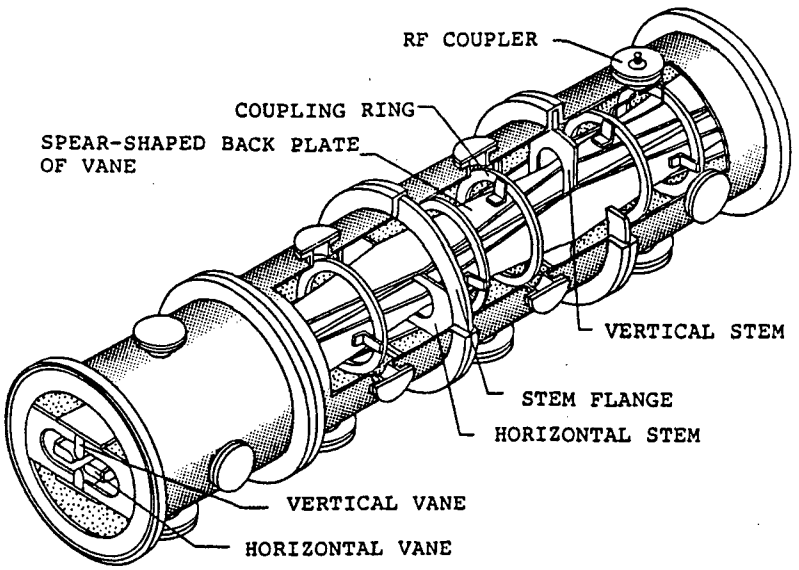

Figure 19: INS Split Coaxial Resonator RFQ Model

The structure illustrated is a 50-MHz test model which has accelerated protons at 1/7th of the design gradient. Table 5 lists the parameters for $q/A = 1/7$ operation. This will be followed by a 25.5-MHz prototype accelerating a $q/A = 1/30$ ion to 45 keV/n, and eventually a full-scale 25.5-MHz machine accelerating a $q/A = 1/60$ ion to 170 keV/n to inject the Japan Hadron Facility with heavy ions.

19 Heavy Ions

Heavy ions present particular difficulties for any accelerator. For an integrated acceleration potential $V = \int E(z)dz$, the energy transferred to the ion with mass A amu is q/A eV per nucleon. Heavy ion velocities in linacs are somewhat lower than for protons (and certainly less than for electrons!). The low velocity results in short accelerating cells.

The minimum length of the accelerating cell in Alvarez linacs is limited by the technology of the magnetic quadrupole that can be placed in the individual drift tubes. At the beginning of the linac, the rf defocusing forces are large, and particularly strong focusing is needed. This limitation forces a high input energy requirement for Alvarez structures.

The RFQ cell length can be made much shorter and the focusing is electrostatic, which is independent of particle velocity. This results in the very low injection energy requirement of RFQs, compared to Alvarez linacs. The RFQ output energy in optimized designs is very compatible with the input energy of Alvarez linacs.

However, even RFQs have a lower limit to the injection energy (velocity) which is further exacerbated by low q/A. Heavy ion RFQs tend to operate at lower frequency to keep the cell length $\beta\lambda/2$ reasonable and keep the aperture a large enough to permit a sufficient transverse acceptance. The focusing strength B, given by Eq. (45), is proportional to q/A of the ion and tends to be low. This limits the acceleration rate, which is proportional to the rf defocusing term Δ given by Eq. (44).

Equally important, the vane tip geometry itself may limit the choice of parameters. The geometry of the vane tip is characterized by the longitudinal curvature in the valleys along the vane, as shown in Figure 6 and given by Eq. (57) for the variable-ρ_t geometry. This minimum longitudinal radius must be kept large enough to allow the vane to be cut by a tool with sufficient size to avoid tool wear and ensure cutting accuracy. For many designs, this represents the most severe constraint.

20 Future Directions

Ten years ago (1980) the RFQ was considered to be an exotic and mysterious device with a mystical design procedure. Now it has matured and driven out the venerable Cockcroft-Walton high voltage preaccelerator as the injector to Alvarez linacs.

The whole book has not yet been written on RFQs, however. Superconducting devices are being modeled at ANL [40], high-average-beam current devices are being developed at various laboratories, and at least one company has now commercialized the device [41], [42]. As with the case of small electron linacs, whose technology has now allowed thousands to be used in hospital-based electron and gamma-ray radiotheraputic applicators, the RFQ may find its way into airport security devices in the form of thermal neutron detection of explosive materials, into small university laboratories for student training and low energy nuclear physics programs, and into applications not yet envisioned.

21 Further Reading

The development of the RFQ has been well documented. The fundamental formulation by LANL appeared in the 1979 Linear Accelerator Conference [10], and sufficient information appears here to develop all the required codes and techniques to get started. A series of comprehensive RFQ tutorials have been given

at several conferences [43], [44], [45], [46], [47].

Any accelerator conference proceedings since 1979 will contain a wealth of information about RFQs, as well as some of the Summer Schools, such as the CERN 1985 School at Queen's College, Oxford [48].

References

[1] I. M. Kapchinskii and V. A. Teplyakov. Linear Ion Accelerator with Spatially Homogeneous Focusing. *Pribory i Tekhnika Eksperimenta 119 No. 2*, pages 19–22, March-April 1970.

[2] J. J. Manca. Some New Accelerating Structures for High Current Intensity Accelerators. Technical Report LA-7157-MS, LANL, 1978.

[3] W. Paul and H. Steinwedel. A New Mass Spectrometer without Magnetic Field. *Z. Naturforschung*, page 448, 1953. No. 8A.

[4] D. H. Sloan and E. O. Lawrence. Production of Heavy High Speed Ions Without High Voltage. *Phys. Rev.*, 38:2021–2032, 1931.

[5] L. W. Alvarez. The Design of a Proton Linear Accelerator. *Phys. Rev.*, 70:799, 1946.

[6] M. Abramowitz and I. A. Stegun. *Handbook of Mathematical Functions.* Dover, 1965.

[7] T. P. Wangler. Space Charge Limits in Linear Accelerators. Technical Report LA-8388, LANL, 1980.

[8] P. M. Lapostolle and A. L. Septier, editors. *The General Theory of Linear Accelerators*, chapter A.2, page 19. North Holland, Amsterdam, 1970.

[9] Lloyd Smith. *Handbuch der Physik, Band XLIV*, chapter Linear Accelerators. Springer, Berlin, 1959.

[10] K. R. Crandall et al. RF Quadruple Beam Dynamics Design Studies. In *Proceedings of the 1979 Linear Accelerator Conference*, pages 205–216, Montauk, N.Y., 1979.

[11] W. D. Kilpatrick. A Criterion for Vacuum Sparking Designed to Include Both R.F. and D.C. Technical Report UCRL-2321, LBL, 1953.

[12] K. R. Crandall. Effects of Vane-Tip Geometry on the Electric Fields in Radio-Frequency Quadrupole Linacs. Technical Report LA-9695-MS, LANL, April 1983.

[13] K. R. Crandall. Proposal for a New Radial Matching Section for RFQ Linacs. Technical Report AT-1:83:3, LANL, 1983.

[14] K. Halbach, R. F. Holsinger, et al. Properties of the Cylindrical RF Cavity Evaluation Code SUPERFISH. In *Proceedings of the 1976 Proton Linear Accelerator Conference*, volume AECL-5677, pages 122–128, Chalk River National Laboratory, 1976.

[15] T. Weiland. On the Unique Numerical Solution of the Maxwellian Eigenvalue Problem in Three Dimensions. *Particle Accelerators*, 17:227–242, 1985.

[16] T. Weiland. Latest Development in Codes for Electromagnetic Fields. In *1988 Linear Accelerator Conference Proceedings*, CEBAF-Report-89-001, pages 273–278, Newport News, Virginia, June 1989.

[17] D. Howard and H. Lancaster. Technique for Stabilizing a Four-Vane Radio Frequency Quadruple Structure. In *Applications of Accelerators in Research and Industry '82*, Denton, Texas, 1982. North Holland.

[18] A. Schempp. Field Stabilisation with Resonant Line Couplers. In *1986 Linear Accelerator Conference Proceedings*, pages 251–253, Stanford, 1986.

[19] E. R. Gray, G. Spalek, and A. H. Shapiro. A Radio-Frequency Quadrupole Accelerator Longitudinal Field Stabilizer. In *1988 Linear Accelerator Conference Proceedings*, CEBAF-Report-89-001, pages 122–124, Newport News, Virginia, June 1989.

[20] M. J. Browman, G. Spalek, and T. C. Barts. Studying the End Regions of RFQ's Using the MAFIA Codes. In *1988 Linear Accelerator Conference Proceedings*, CEBAF-Report-89-001, pages 64–66, Newport News, Virginia, June 1989.

[21] R. M. Hutcheon and G. E. McMichael. Low Power RF Tuning of the RFQ1 Accelerator. In *1988 Linear Accelerator Conference Proceedings*, CEBAF-Report-89-001, pages 94–96, Newport News, Virginia, June 1989.

[22] T. P. Wangler. Physics Design of Linear Accelerators for Intense Ion Beams. In *1988 Linear Accelerator Conference Proceedings*, CEBAF-Report-89-001, pages 211–215, Newport News, Virginia, June 1989.

[23] I. Kapchinskii and V. Vladimirskii. Limitations of Proton Beam Current in a Strong Focusing Linear Accelerator Associated with the Beam Space Charge. In *Second International Conference on High Energy Accelerators*, page 274, CERN, 1959.

[24] K. R. Crandall. Private Communication.

[25] O. R. Sander, F. O. Purser, and D. P. Rusthoi. Operational Parameters of a 2.0-MeV RFQ Linac. *Proceedings of the 1984 Linear Accelerator Conference*, GSI-84-11:54, 1984.

[26] D. Schrage et al. A Flight-Qualified RFQ for the BEAR Project. *1988 Linear Accelerator Conference Proceedings*, pages 54–57, June 1989.

[27] J. W. Staples et al. Initial Operation of the New Bevatron Local Injector. In *1985 Particle Accelerator Conference*, volume NS-32, No. 5, pages 3208–3209, Vancouver, 1985.

[28] J. W. Staples. Beam Dynamics and Vane Geometry in the LBL Heavy Ion RFQ. In *1983 Particle Accelerator Conference*, volume NS-30, No. 4, pages 3533–3535, Santa Fe, 1983.

[29] H. Haseroth, C. Hill, P. Tetu, M. Weiss, B. H. Wolf, K. Leible, P. Spadtke, J. Klabunde, B. Langenbeck, N. Angert, R. A. Gough, J. Staples, R. Caylor, D. Howard, R. MacGill, and J. Tanabe. Ion Acceleration in the CERN Linac. In *1986 Linear Accelerator Conference Proceedings*, volume SLAC-303, pages 355–357, Stanford, 1986.

[30] R. A. Gough, J. Staples, J. Tanabe, D. Yee, D. Howard, C. Curtis, and K. Prelec. Design of an RFQ-Based H^- Injector for the BNL/FNAL 200 MeV Proton Linac. In *1986 Linear Accelerator Conference Proceedings*, volume SLAC-303, pages 260–262, Stanford, 1986.

[31] J. G. Alessi et al. Performance of the New AGS RFQ Preinjector. In *Proceedings of the 1989 Particle Accelerator Conference, 89CH2669-0*, pages 999–1001, Chicago, 1989.

[32] S. Abbott, R. MacGill, and R. Yourd. Mechanical Design of a Heavy Ion RFQ. In *1983 Particle Accelerator Conference*, volume NS-30, No. 4, page 3004, Santa Fe, 1983.

[33] S. Abbott et al. Design of an Integrally Formed RFQ. In *Proceedings of the 1989 Particle Accelerator Conference, 89CH2669-0*, pages 953–955, Chicago, 1989.

[34] E. L. Kemp, D. J. Liska, and M. D. Machalek. The Fusion Materials Irradiation Test (FMIT) Accelerator. In *Proceedings of the 1979 Linear Accelerator Conference*, volume BNL-51134, page 21, Montauk, N.Y., 1979.

[35] G. M. Arbique, B. G. Chidley, G. E. McMichael, and J. Y. Sheikh. CW Operation and Initial Beam Experiments with the RFQ1 Accelerator. In *1988 Linear Accelerator Conference Proceedings*, CEBAF-Report-89-001, page 91, Newport News, Virginia, June 1989.

[36] G. E. McMichael et al. Exploring the Beam Parameter Space of a CW RFQ Proton Accelerator. In *Proceedings of the 1989 Particle Accelerator Conference, 89CH2669-0*, pages 980–982, Chicago, 1989.

[37] A. Schempp. 4 Rod RFQ for the GSI Linac. In *Proceedings of the 1989 Particle Accelerator Conference, 89CH2669-0*, volume 89CH2669-0, pages 1093–1097, Chicago, 1989.

[38] I. M. Kapchinskiy et al. RF Linac for Heavy Ion Fusion Driver. In *1986 Linear Accelerator Conference Proceedings*, volume SLAC-303, pages 318–322, Stanford, 1986.

[39] E. Tojyo, S. Arai, T. Fujino, T. Fukushima, and N. Tokuda. A Multi-Module Cavity Structure of Split Coaxial RFQ. In *1986 Linear Accelerator Conference Proceedings*, volume SLAC-303, pages 374–376, Stanford, 1986.

[40] J. R. Delayen. Superconducting Accelerating Structures for High-Current Ion Beams. In *1988 Linear Accelerator Conference Proceedings*, CEBAF-Report-89-001, pages 122–124, Newport News, Virginia, June 1989.

[41] R. J. Hamm. Linacs for Medical and Industrial Applications. In *1986 Linear Accelerator Conference Proceedings*, volume SLAC-303, pages 33–36, Stanford, 1986.

[42] R. J. Hamm, K. R. Crandall, M. E. Hamm, L. D. Hansborough, and J. M. Potter. A Compact Proton Linac for Positron Tomography. In *1986 Linear Accelerator Conference Proceedings*, volume SLAC-303, pages 141–143, Stanford, 1986.

[43] H. Klein. Development of the Different RFQ Accelerating Structures and Operation Experience. In *1983 Particle Accelerator Conference*, volume NS-30, No. 4, pages 3313–3322, Santa Fe, 1983.

[44] S. Schriber. Present Status of RFQ's. In *1985 Particle Accelerator Conference*, volume NS-32, No. 5, pages 3134–3138, Vancouver, 1985.

[45] J. W. Staples. RFQ's In Research and Industry. In *1986 Linear Accelerator Conference Proceedings*, volume SLAC-303, pages 227–231, Stanford, 1986.

[46] A. Schempp. Recent Progress in RFQ's. In *1988 Linear Accelerator Conference Proceedings*, CEBAF-Report-89-001, pages 460–464, Newport News, Virginia, June 1989.

[47] J. G. Alessi. RFQ Preinjectors. In *Applications of Accelerators in Research and Industry '88*, pages 954–958, Denton, Texas, 1988. North Holland.

[48] M. Puglisi. The Radiofrequency Quadrupole Linear Accelerator. In *CERN Accelerator School Advanced Accelerator Physics, September 1985*, volume CERN 87-03, The Queens's College, Oxford, England, April 1987.

LAWRENCE BERKELEY LABORATORY
UNIVERSITY OF CALIFORNIA
INFORMATION RESOURCES DEPARTMENT
BERKELEY, CALIFORNIA 94720